



# Effects of porosity and composition on seismic wave velocities and elastic moduli of lower cretaceous rocks, central Lebanon

Mohamed K. Salah<sup>1</sup> · Mohammad Alqudah<sup>1,2</sup> · Ahmad K. Abd El-Aal<sup>3,4</sup> · Christophe Barnes<sup>5</sup>

Received: 23 November 2017 / Accepted: 1 August 2018 / Published online: 16 August 2018  
© Institute of Geophysics, Polish Academy of Sciences & Polish Academy of Sciences 2018

## Abstract

We collected 40 rock samples from the Cretaceous strata exposed at central Lebanon in order to study the effects of porosity and rock composition on their seismic wave velocities and elastic moduli. Several sedimentological and mineralogical studies were conducted to evaluate the rock composition, provenance, depositional conditions, and the diagenetic history of the studied rocks. Porosity, bulk and grain densities and seismic wave velocities were measured for 35 drilled core samples at ambient conditions in the laboratory. Velocity measurements were conducted on the dry core samples utilizing the pulse transmission technique. Petrographically, four lithofacies have been identified under the polarizing microscope. From oldest to youngest, these comprise arenitic sandstone, lithic limestone, oolitic limestone, and micritic limestone. Investigations of representative rock samples under the SEM revealed that a number of diagenetic processes have impacted the studied rocks, and thereby affected their petrophysical properties. The XRD analysis, on the other hand, revealed that quartz and calcite are the dominant minerals in the sandstones of the Chouf Formation and the limestones of the Abeih and Mdairej Formations, respectively. The measured porosity, bulk density, and compressional and shear wave velocities of the investigated rocks vary, respectively, between 2.14–10.05%, 2.41–2.67 g/cm<sup>3</sup>, 3885–6385 m/s and 2246–3607 m/s. The grain density was calculated from the measured porosity and bulk density data and varies narrowly between 2.64 and 2.78 g/cm<sup>3</sup>. We further calculated the Poisson's ratio and the moduli of shear, bulk, and Young from the measured bulk density and seismic wave velocities. Calculated values of these parameters vary between 0.18–0.28,  $1.23\text{--}3.43 \times 10^{10}$  Pa,  $2.03\text{--}6.18 \times 10^{10}$  Pa and  $3.06\text{--}8.69 \times 10^{10}$  Pa, respectively. The generalized mixture rule is used to provide a unified description of the physical properties of the studied rocks regarding their component properties, volume fractions, and microstructures. We constructed a number of relationships between the measured petrophysical and elastic properties to evaluate the mutual interdependence of these parameters and assess the effects of porosity and rock type on these important rock characteristics.

**Keywords** Petrophysics · Seismic wave velocities · Elastic moduli · The generalized mixture rule (GMR) · Cretaceous rocks · Central Lebanon

✉ Mohamed K. Salah  
ms264@aub.edu.lb

<sup>1</sup> Department of Geology, American University of Beirut, Riad El Solh, Beirut 1107 2020, Lebanon

<sup>2</sup> Geology Department, Faculty of Science, Yarmouk University, Irbid 21163, Jordan

<sup>3</sup> Civil Engineering Department, Faculty of Engineering, Najran University, P.O. Box 1988, Najran, Saudi Arabia

<sup>4</sup> Geology Department, Faculty of Science, Assiut Branch, Al Azhar University, Cairo, Egypt

<sup>5</sup> Department of Geosciences and Environment, University of Cergy-Pontoise, 95031 Cergy-Pontoise, France

## Introduction

Seismic wave velocities (mainly the primary and secondary wave velocities, denoted here as  $V_p$  and  $V_s$ , respectively) are essential parameters controlling the mechanical properties of many substances (e.g., Wang et al. 2009). The  $V_p$ ,  $V_s$  and the bulk density ( $\rho_b$ ) are the input data required to calculate the different elastic moduli of a rock, and are, therefore, fundamental for characterizing Earth materials. Knowledge of these physical parameters along with the effects of rock porosity on them are essential for a wide range of applications including seismic hazard estimation, understanding geological structures, faulting mechanism, source properties, and the evaluation of strong ground motions (Wang et al. 2009).

Lithology, lithostatic pressure, clay content, degree of fracturing and other structural and textural properties have a great effect on seismic wave velocity (e.g., Kassab and Weller 2013, 2015). Moreover, diagenesis has a great effect on porosity and other rock properties which in turn will affect the elastic properties of rocks. It may diminish or enhance the porosity and, therefore, affects significantly the mechanical strength of Earth materials and the quality of reservoir rocks and aquifers. Practically, rocks are not composed totally of grains; rather, a certain amount of voids and/or fractures always exist allowing fluids to flow within the rock body. Both pore volume and fluid flow (i.e., porosity and permeability) have great effects on the strength and physical properties of rocks (Chen et al. 2005; Yu et al. 2016).

The elastic properties of rocks can be described by any two of four elastic constants which comprise the shear modulus ( $\mu$ ), the bulk modulus ( $\kappa$ ), the Young's modulus ( $E$ ), and the Poisson's ratio (e.g., Yu et al. 2016). These elastic constants are strongly affected by the porosity ( $\phi$ ), and accordingly,  $V_p$  and  $V_s$  vary also with  $\phi$  (Han et al. 1986; Cadoret et al. 1995; Han and Batzle 2004). Little studies have been done on the effects of porosity on Poisson's ratio ( $\sigma$ ), which is calculated from seismic velocities, because of a lack in experimental data over wide ranges of porosities and pore geometry (e.g., Salem 2000). Thus, it is important to explore the relationship between seismic wave velocity and  $\phi$  in sedimentary rocks. In reality, such target has been an important area of research for several decades (e.g., Wyllie et al. 1956, 1958; Knackstedt et al. 2005; Ji et al. 2007, 2018; Yu et al. 2016). In well logs, for example, such relations are regarded as additional controls on inferring porosity from sonic logging and in situ indicators of fluid types (Dvorkin and Nur 1998). Moreover, our current knowledge on the seismic wave dependence on porosity are limited and obtained only from surface outcrops and rock samples obtained from

mining and drilling which, at maximum, comprise only the top 10–12 km (Yu et al. 2016). Much of our knowledge about the Earth's interior comes mainly from seismic data. In addition to phase transformations at major discontinuities, chemical composition, metamorphic and dehydration reactions, pressure/temperature regimes, and partial melting, porosity is a critical parameter affecting the elastic properties of both dry and wet rocks (Ji et al. 2002). The assessment of the porosity effects on the seismic wave velocities in rocks is, however, a challenging task because the pore geometry, size distribution and connectivity of pores in rocks are usually unclear.

Since early times, various researchers have investigated the relationship between  $V_p$  and  $\phi$  and presented a number of empirical equations for different geologic settings containing different types of deposits (e.g., Wyllie et al. 1956, 1958; Gardner et al. 1974; Raymer et al. 1980; Castagna et al. 1985; Hyndman et al. 1993; Erickson and Jarrad 1998; Vernik et al. 2002; Dutta et al. 2009; Ojha and Sain 2014). Empirical relationships remain most popular because they represent actual laboratory or log measurements (Knackstedt et al. 2005). However, measured porosity–velocity data show usually a high degree of scatter, which results mainly from variations in lithology, pore geometry, pore size, shape, degree of compaction, cementation, clay content, and distribution (Han et al. 1986; Marion et al. 1992). Thus, experimental data are usually grouped into categories of different lithologies such as limestones, dolostones, sandstones, shaly sands, and shales (Nur et al. 1995; Wang 2000). Wyllie et al. (1956) equation, for example, is valid for the estimation of the porosity of sandstones from sonic logs. The equation of Raymer et al. (1980), which is an improved version of the Wyllie et al. (1956) time-average equation, can be effectively used to relate  $V_p$  to  $\phi$  in cemented, saturated, sandstones through a wide porosity range. Kitamura et al. (2005) recognized that seismic velocities decrease from siltstone to sandstone at low fluid pressure. In the laboratory experiments conducted by Castagna et al. (1985) on different rocks, decreases of both  $V_p$  and  $V_s$  with increasing  $\phi$  have been observed. Moreover, data analysis performed by Wang et al. (2009) showed that any change in  $\phi$  induces similar changes in the seismic wave velocities. However, empirical relationships can seldom be applied outside the range of measured data; hence the study of the porosity–velocity relationship for different geological settings containing specific lithologies is essential. In the present analysis, we will use the generalized mixture rule (GMR; Yu et al. 2016) to give a systematic framework expressing the variations of the elastic moduli ( $\mu$ ,  $\kappa$ , and  $E$ ), and seismic velocities ( $V_p$  and  $V_s$ ) as a function of porosity of the studied rocks.

In this study, we have collected 40 rock samples from the lower Cretaceous Formations exposed at central Lebanon to investigate their lithologic and petrophysical characteristics with some focus on the effects of porosity and rock type on the seismic wave velocities and elastic moduli. Lithologically, these formations are dominated by sandstones and carbonates which usually have a diagenetically induced porosity. These rocks have not been previously studied in detail and, therefore, the present investigation provides an important database for interested researchers. In addition, recent seismic exploration activities in the region confirmed the large sedimentary thickness and strong potential of the Mesozoic and Cenozoic strata (Bou Daher et al. 2016). Given these new hydrocarbon discoveries in the Oligocene and Miocene reservoirs in the eastern Mediterranean region (Esestine et al. 2016), it became essential to evaluate the petroleum system in the area and estimate the quality of the encountered formations. Carbonate rocks are valuable in many industrial and engineering applications and have significant contributions to the national economy of many countries (Ersoy et al. 2016). Since the majority of the investigated rocks are mainly carbonates, this adds to the significance of the present study. We investigate the porosity dependence of  $\rho_b$  for the studied rocks and their elastic properties including  $V_p$ ,  $V_s$ ,  $\sigma$ , and the three elastic moduli  $\mu$ ,  $\kappa$ , and  $E$ . We then compare our results with those obtained by different researchers at a number of geologic settings. We classify the measured porosity as primary or secondary based on its origin and assess the effects of the rock composition and the different diagenetic processes such as compaction and lithification on porosity and, in turn, on the elastic properties of the investigated formations.

## Geologic setting and stratigraphy

The Levant was formed as a result of an extensional rifting of the northern margin of Gondwana which started in the Late Paleozoic (Garfunkel 1989; Hawie et al. 2013; Nader 2014), and probably continued until the Late Jurassic (Gardosh et al. 2010). These rift phases were followed by a phase of cooling and subsidence until the Late Cretaceous. The convergence between the Afro-Arabian and Eurasian plates and the consequent closure of the Neotethys Ocean (Fig. 1) started in the Late Cretaceous (Bou Daher et al. 2016). The eastern margin of the Levant is bounded by a series of strike–slip faults formed as a northward extension of the Red Sea rifting which started in the Oligocene/Miocene times. These strike–slip faults represent the Levant Fracture System (LFS; Fig. 1), which extends from the Gulf of Aqaba in the south to the Taurus Mountains in the north (Beydoun 1999). Due to the differential

northward motion of both the African and the Arabian plates, with the latter being faster (McClusky et al. 2000), the LFS is a sinistral strike–slip fault involving the N–S striking Dead Sea Fault Zone in the south, the central NNE–SSW trending segment (Yammouneh Fault and splays), and again the N–S striking Ghab Fault in the north (Ghalayini et al. 2014). These three segments are known together as the Dead Sea Fault Zone, which extends northward until it meets the East Anatolian Fault Zone in southern Turkey (Fig. 1). The Lebanese segment of the LFS is very complex and is divided into many branches and veers to the right forming a restraining bend which led to the formation of the high reliefs of Mount Lebanon (Daëron et al. 2007).

The Mesozoic stratigraphic section of onshore Lebanon is dominated by carbonates (Nader 2014) although some clastics are also encountered (Fig. 2). Accumulation of sediments in the Levant was almost continuous, but, in the margin and onshore Lebanon, many erosional events are detected (Müller et al. 2010; Hawie et al. 2014). The uplift of both the Mount Lebanon and Anti-Lebanon, resulting from transpressive regime at the Lebanese segment of the LFS, induced the latest ongoing erosional event (Beydoun 1999; Gomez et al. 2006). Many episodic volcanic eruptions are recorded in the eastern Mediterranean such as the northern Lebanon alkaline volcanism during the Late Jurassic–Early Cretaceous (Nader 2014). This intermittent volcanic activity is induced by a mantle plume activity in the Levant (e.g., Garfunkel 1992; Wilson 1992).

Early Cretaceous strata in Lebanon are represented mainly by four geologic formations. In an ascending order they are the Chouf Formation (mainly sandstone), the Abeih Formation, the Mdairej Limestone Formation, and the Hammana Formation (Walley 1983). Because of some field obstacles, we collected rock samples from the first three formations at five field sites (Fig. 3). The Chouf Formation is named after the Chouf region of southern central Lebanon where the thickest sandstones are exposed. These sandstones are ferruginous, cross-bedded, multicolored, and vary in grain size from fine to medium (Fig. 4a–c). They are sometimes associated with clays, shales, and lignites (Walley 1997, 1998). The darker layers may contain woody or coaly fragments associated with pyrite, marcasite, and amber. The upper limit of these sandstones is marked by a layer of abundant oysters which is the base of the Abeih Formation. The age of the Chouf Formation is Berriasian to Hauterivian and has an average thickness of 220 m in its type locality, although it may reach up to 300 m in some areas reflecting syn-depositional block faulting.

The overlying Abeih Formation consists of fossiliferous massive limestones with common marls and thin sandstone beds especially at its lower base (Figs. 2, 4a, d, e). This

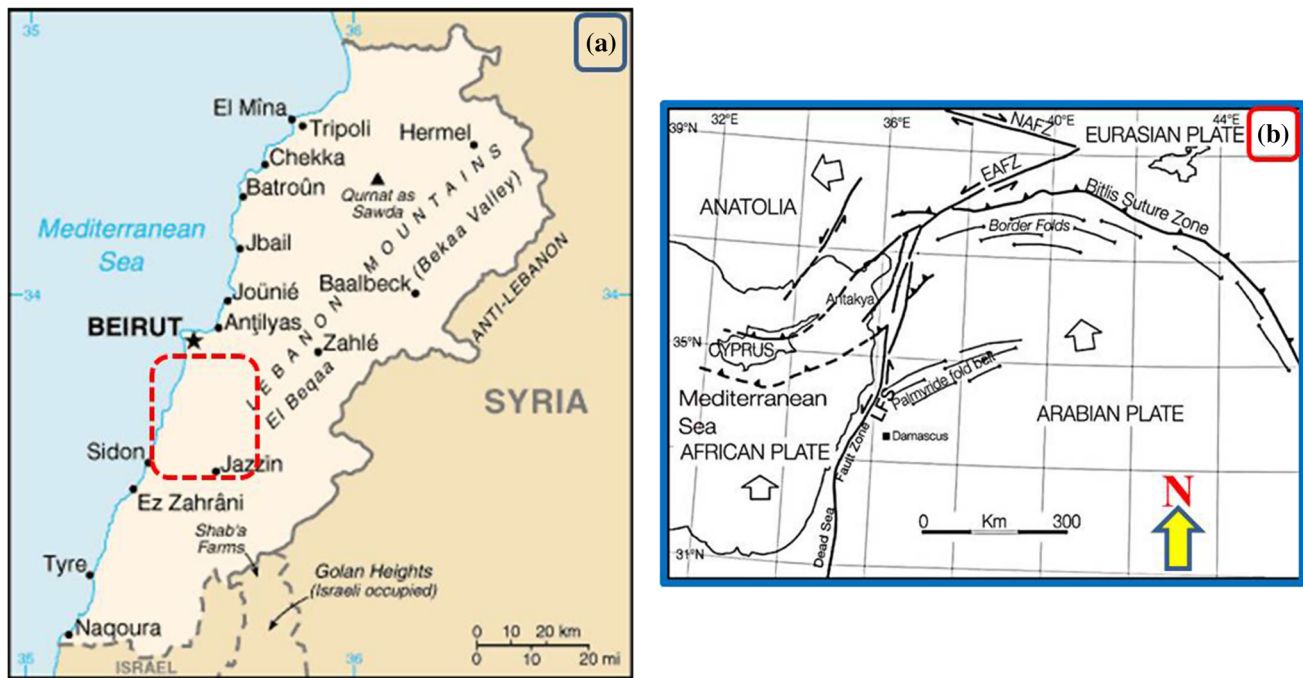


**Fig. 1** Geographic map of Lebanon in the eastern Mediterranean with a red rectangle marking the present study area (a) and a tectonic map of the eastern Mediterranean region showing the major neotectonic lineaments in the vicinity of the junctions between the Eurasian, African and Arabian plates and the Anatolian collage (b). White

arrows in (b) denote the present-day plate motions. *LFS* Levant Fracture System, *EAFZ* East Anatolian Fault Zone, *NAFZ* North Anatolian Fault Zone. Reproduced with permission from Tatar et al. (2004)

formation is overlain by the thick massive limestones of the Mdairej Formation and attains an average thickness of 170 m in the Chouf area (Walley 1997). The age of the lower part of the Abeih Formation is Barremian, whereas the upper part is thought to be of earliest Aptian age. The overlying distinct limestone cliffs constitute the Mdairej Formation which is clearly recognizable as a sheer-sided cliff (Fig. 5a–e). The basal section of this formation is ferruginous calcarenite which changes upward to the finely massive, bedded, pale gray, limestone (Walley 1997). This formation is partially dolomitized with rare macrofossil content. The upper limit of this formation is located where the massive reddish brown limestones are overlain by green clays. Its thickness is about 50 m and is of lower Aptian age.

## Materials and methods

### Petrography and mineralogy

A total of 14 representative thin sections were investigated under the polarizing microscope to identify the mineralogical composition, microfacies associations, the different diagenetic processes, and the thin-section porosity of the samples. Standard microfacies types were assigned to

each sample according to Wilson (1975) and Flügel (1982). Different lithologies such as micritic limestone, lithic limestone, oolitic limestone, and arenitic sandstone have been identified. Porosity assignment follows the method of Scholle and Ulmer-Scholle (2003) and Selley and Sonnenberg (2015). Many features that characterize porosity and the paleo-environment were also investigated during the petrographic study of the thin sections. These features comprise: (1) grain types; bioclasts/non-bioclasts ratio (for the carbonate facies), or, the major and minor components for the clastic rocks; (2) type of porosity; (3) cement, matrix content and their types; (4) the rock texture; including roundness, sphericity, sorting, grain size and grain packing; and (5) any diagenetic feature. Sorting percentage is estimated following Longiaru (1987), whereas the bioclast/non-bioclast ratio is determined after Baccelle and Bosellini (1965). Microscopic images were taken from thin sections using Fuji light microscope attached with a digital camera. On the other hand, the scanning electron microscope (MIRA3 LMU) with OXFORD EDX detector was used to acquire the SEM images by TESCAN on small cuts in the Central Research Science Laboratory (CRSL) of the American University of Beirut. To confirm the mineral composition of the studied rocks, a total of 32 representative samples were crushed and prepared as powders for testing under the



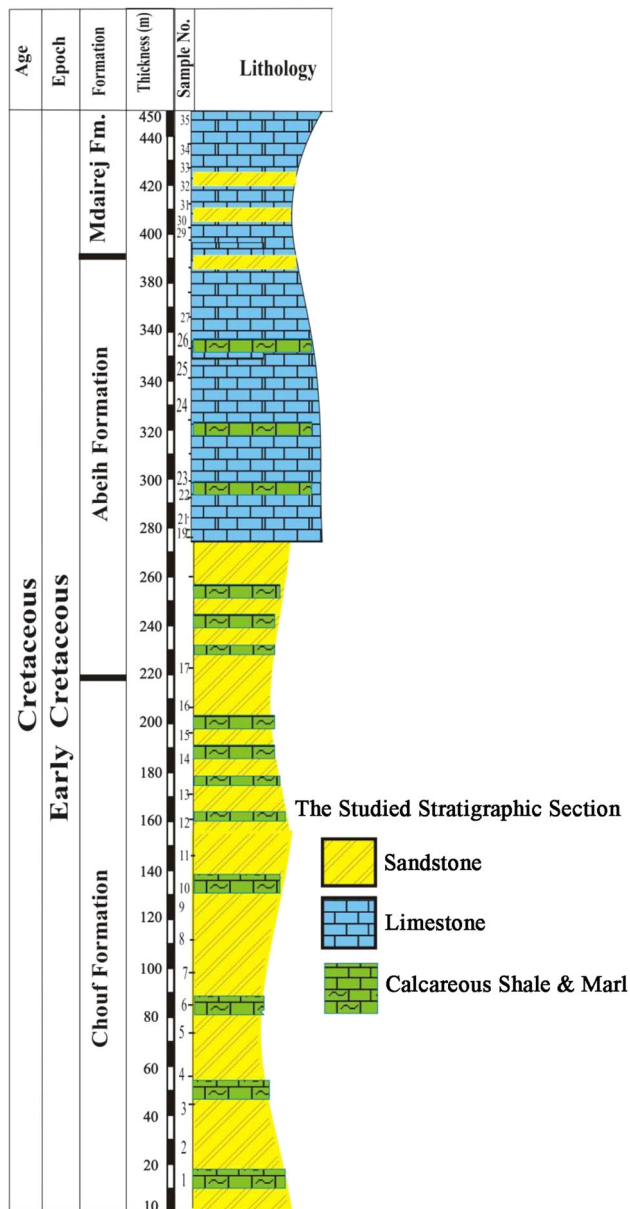


**Fig. 2** A stratigraphic columnar section of the three investigated Early Cretaceous Formations in *central Lebanon* showing their lithology and sample locations. Modified after Walley (1983, 1997)

BRUKER D8 advanced X-ray diffractometer (XRD) also in the CRSL of the American University of Beirut.

### Core analysis

Routine core analysis is a critical part of an overall rock evaluation as it provides direct estimation of the rock properties and is a mean to calibrate other assessment tools such as well logs and surface geophysics (Eysa et al. 2016). A total of 35 one-inch-diameter cores were obtained from the exposed rocks in the field which represent the three studied formations (Fig. 6). Sampling in the field was

accomplished using a gasoline-powered portable rock core driller (Model D261-C), where core samples of one-inch-diameter can be obtained (Fig. 6b–d). Core samples were later sliced in the lab to lengths of 2–5 cm (depending on the initial core length obtained in the field) to remove the weathered surface and flatten the core ends for accurate cross-sectional area and bulk volume determination (Fig. 6d). The cores were first dried at a temperature of 100 °C to remove any moisture and weighed (Fig. 6e) and then analyzed using Automated Permeameter–Porosimeter (AP-608). The AP-608 is a state-of-the-art system for measuring gas permeability and porosity of core samples under various pressure conditions (in our case three test pressures were applied to each sample: 500 psi, 850 psi and 1200 psi). Using the core length and diameter, the bulk volume ( $V_b$ ) was calculated and used in the determination of porosity and bulk density. Boyle’s Law is concerned with the ability to determine an unknown volume by expanding a gas of known pressure and temperature conditions into a void space of known volume and using the resulting pressure to calculate the unknown volume. The grain volume ( $V_g$ ) of the sample is calculated as follows:

$$V_g = V_c - V_r[(P_1 - P_2)/P_2 - P_a] + V_v[P_2/(P_2 - P_a)] \quad (1)$$

where  $V_c$ , sample chamber volume;  $V_r$ , reference chamber volume;  $V_v$ , valve displacement volume;  $P_1$ , absolute initial reference volume pressure;  $P_2$ , absolute expanded pressure;  $P_a$ , absolute atmospheric pressure initially in sample chamber.

In general, effective porosity can be determined if any two of three related volumes; namely the bulk volume, interconnected pore volume ( $V_{pr}$ ), and the grain volume are known where:

$$V_b = V_{pr} + V_g. \quad (2)$$

Once the sample bulk volume and grain volume are known, then we can readily determine the volume of pores ( $V_{pr}$ ), from which the sample porosity ( $\phi$ ) can be estimated from the following simple form:

$$\phi = V_{pr}/V_b. \quad (3)$$

The bulk density ( $\rho_b$ ) is the mass per unit volume of a rock in its natural state. It is equal to the mass of the dry rock sample ( $M_d$ ) divided by its bulk volume.

$$\rho_b = M_d/V_b \quad (4)$$

In addition, the grain density ( $\rho_g$ ) can be determined as follows:

$$\rho_g = M_d/V_g. \quad (5)$$

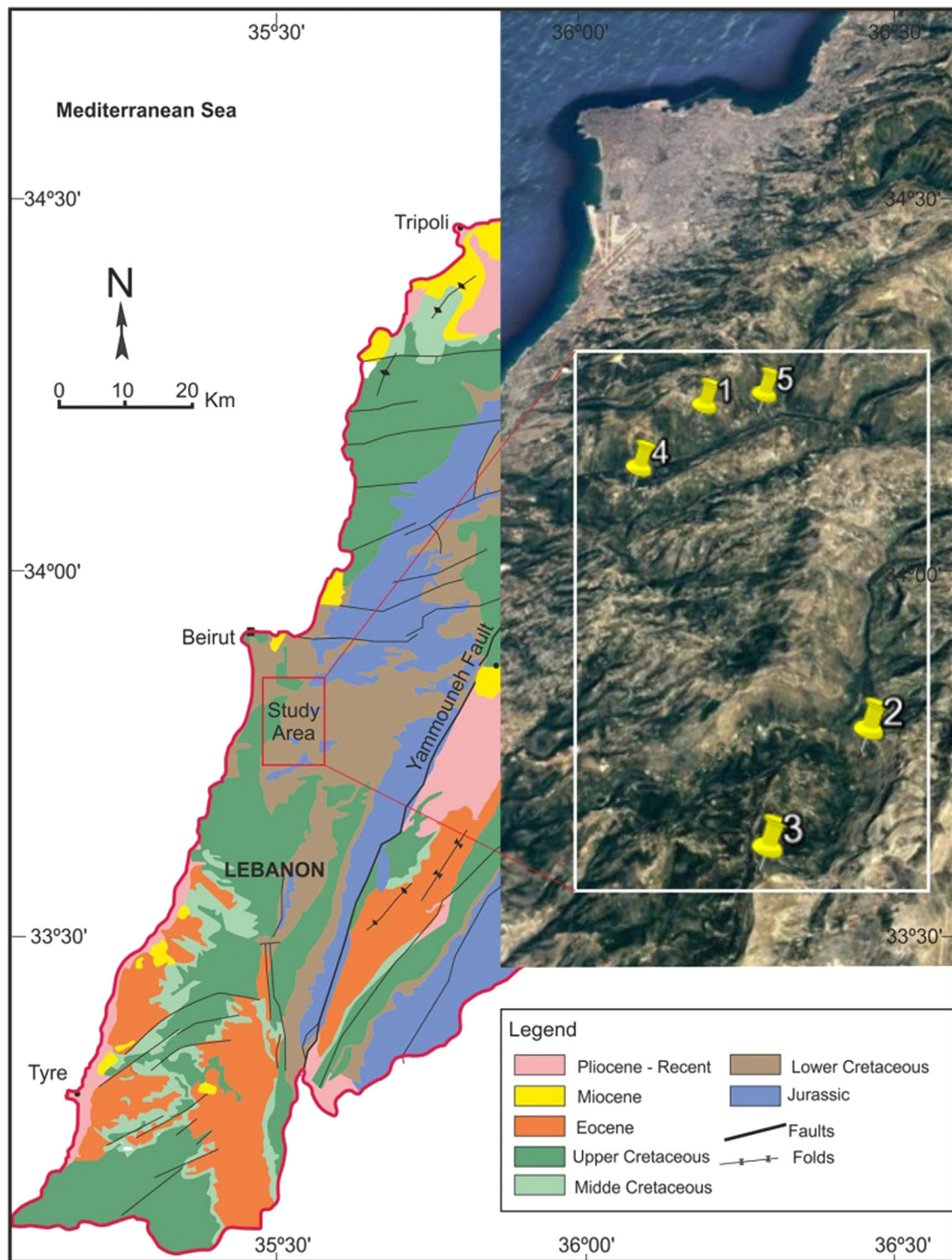


**Fig. 3** Geological map of Lebanon (modified after Dubertret 1955), with an inset showing the sampling locations at the study area which are given serial numbers indicating the order of successive five field visits

### Acoustic velocities

The measurements of seismic wave velocities can be conducted both in situ and in the laboratory. The acoustic

wave velocity analysis is highly significant, nondestructive, test that is relatively easy to apply and is, therefore, increasingly used in many geological and geotechnical applications. It is used specifically in civil engineering and



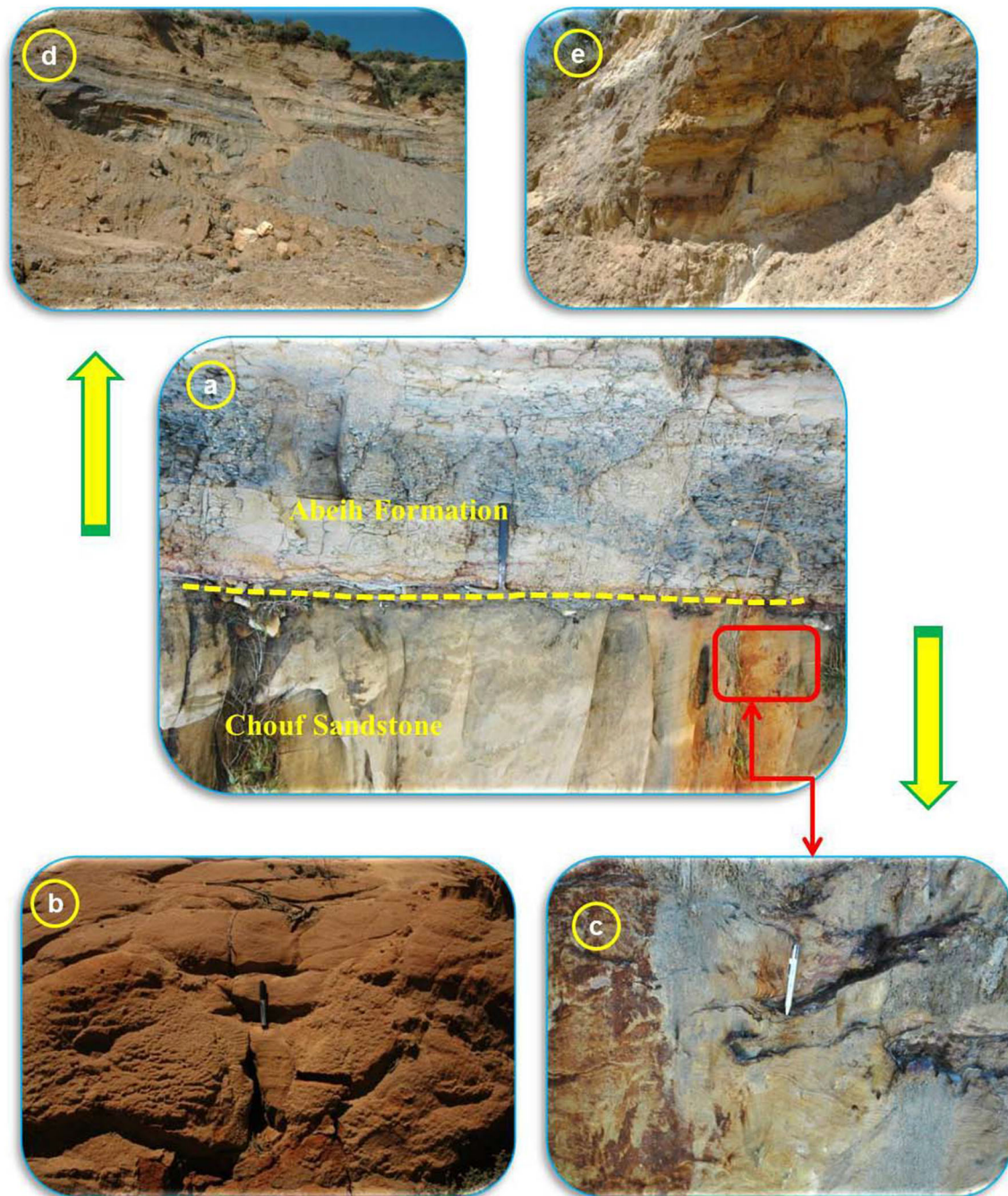


**Fig. 4** Field photographs showing the contact between the Chouf and Abeih Formations (a) with sandstone exposures from the Chouf Formation (b, c) and marl and limestone outcrops from the Abeih Formation (d, e)

mining projects such as underground opening, quarrying, blasting, and ripping (Singh et al. 2004; Kahraman and Yeken 2008). Moreover, seismic data are very vital in the field of hydrocarbon exploration and production (e.g., Sønneland and Barkved 1990; Anselmetti and Eberli 1999; Stewart et al. 2000; Baechle et al. 2004; Eberli et al. 2004; Ngoc et al. 2014; Onajite 2014; Nanda 2016).

The velocity of ultrasonic pulses traveling in a solid material is controlled by many factors including the mineral composition, texture, density, porosity, pore water, confining pressure, temperature, weathering and alteration, bedding planes, joint properties (roughness, filling material, water, attitude, etc.), and anisotropy (Sharma and Singh 2008). For example, the extensive research done by Birch (1960), Gardner et al. (1965), Christensen (1974),



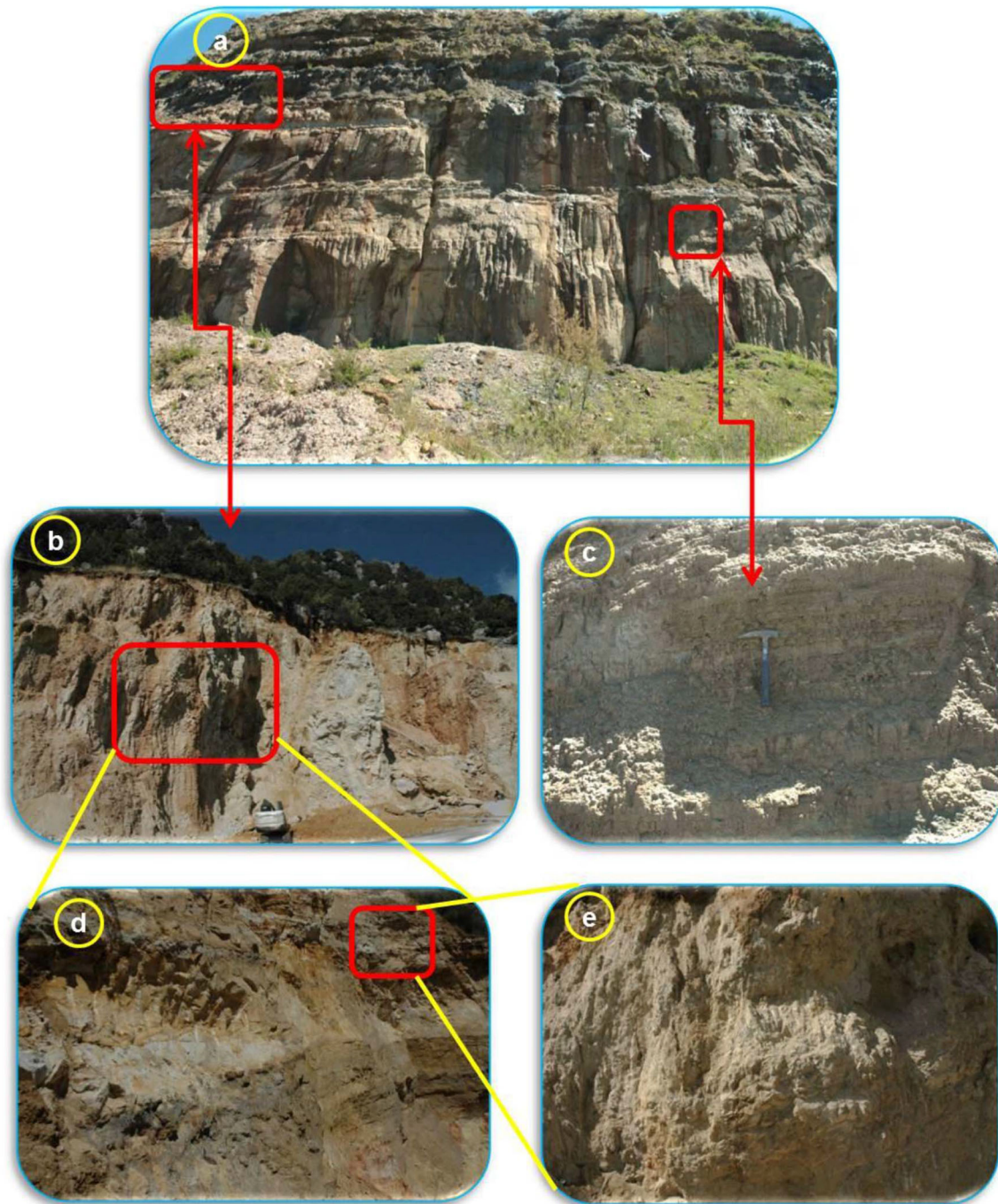


**Fig. 5** Field photographs showing the exposed limestone outcrops of the Abeih Formation and the high cliffs of the gray limestones of the Mdairej Formation (a–e)

Eberhart-Phillips et al. (1989), Wepfer and Christensen (1991), Freund (1992), Greenfield and Graham (1996), Ji and Wang (1999) and Ji et al. (2007), beside others, on a variety of rock samples revealed the velocity dependence on the confining pressure applied to the studied rocks. In the present study, the pulse transmission technique of velocity measurements (at a frequency of 1 MHz) at the CoreLab, Texas, USA, was used to measure the  $V_p$  and  $V_s$

of the dry core samples at room temperature and ambient pressure. Since the rock samples of our study are collected from exposed rocks, we measured the seismic wave velocities under ambient pressure conditions. Two transducers are attached tightly to the sample ends until the arriving signal stabilizes ensuring a good contact between them and the sample surfaces.



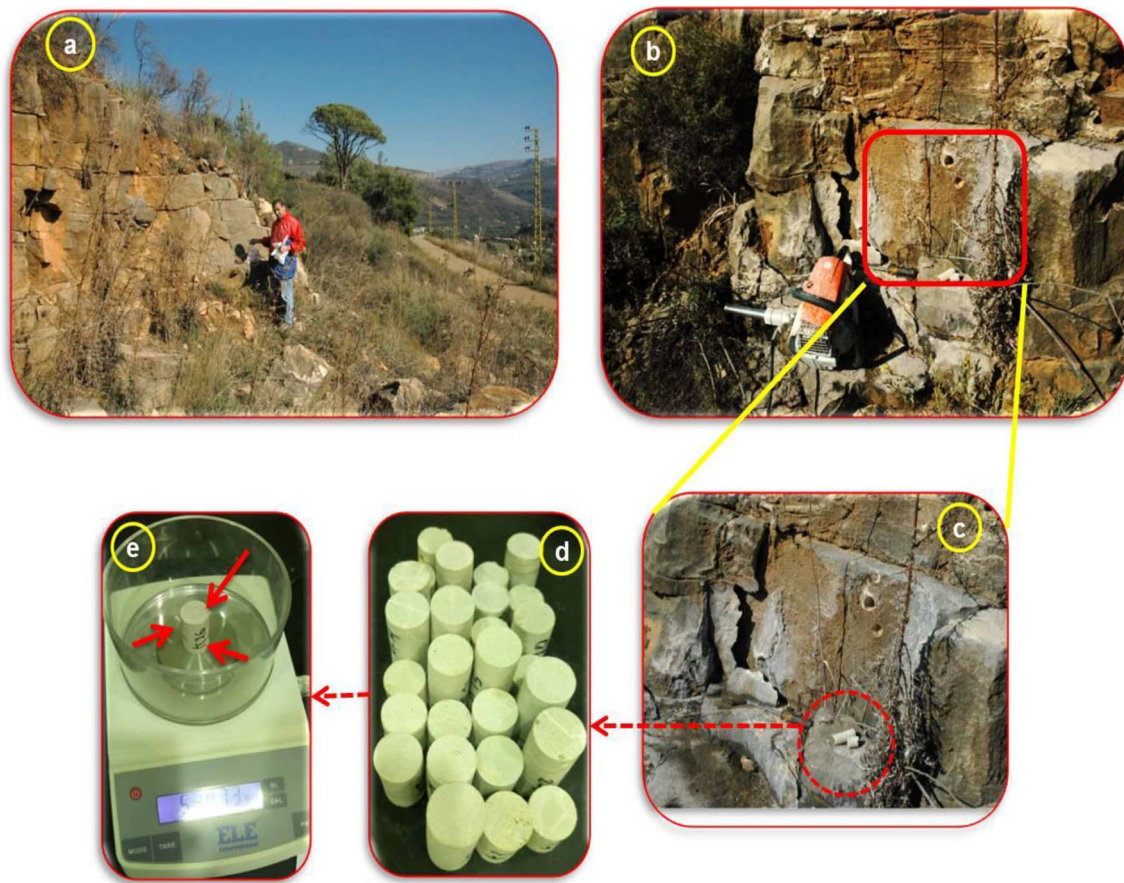


**Fig. 6** Field photographs showing how the core samples are collected from the studied outcrops in the field (a–c) and consequent preparation (d) and sample weighing (e) with an electronic balance

Dynamic elastic parameters (the shear, bulk, Young moduli, and the Poisson's ratio) were calculated using the measured  $V_p$ ,  $V_s$ , and the  $\rho_b$  of the sample based on the linear elastic theory. The following equation is used to calculate  $\sigma$ :

$$\sigma = (V_p^2 - 2V_s^2) / 2(V_p^2 - V_s^2). \quad (6)$$

The shear ( $\mu$ ), bulk ( $\kappa$ ), and Young ( $E$ ) moduli are also calculated from the measured seismic wave velocities (e.g., Russell and Smith 2007) and  $\rho_b$  as follows:

$$\mu = \rho_b V_s^2 \quad (7)$$

$$\kappa = \rho_b (V_p^2 - (4/3)V_s^2) \quad (8)$$

$$E = \rho_b V_s^2 \left( (3V_p^2 - 4V_s^2) / (V_p^2 - V_s^2) \right). \quad (9)$$

The shear modulus is defined as the resistance of a material to a simple shear strain that is changing the material shape without any volume change, whereas the bulk modulus measures the resistance of a substance to uniform compression. The Young's modulus, on the other hand, is the ratio between the stress acting along an axis

and the resulting strain along the same axis within the range of uniaxial stresses in which Hooke's law is valid (Yu et al. 2016). Finally, Poisson's ratio is the negative of the ratio between the transverse strain and the axial strain if an isotropic material is stressed uniaxially (e.g., Christensen 1996; Gercek 2007; Timoshenko and Goodier 1970; Wang and Ji 2009; Ji et al. 2018). Although theoretically  $\sigma$  can range from  $-1.0$  to  $0.5$  (e.g., Ji et al. 2010), most materials exhibit a positive  $\sigma$  which means that they expand in directions orthogonal to the applied stress (Ji et al. 2018). This parameter provides better constraints on the petrological composition and properties of rocks than the  $V_p$  and  $V_s$  by removing the non-uniqueness in velocity interpretation (e.g., Christensen 1996; Wang and Ji 2009). The measured and calculated petrophysical parameters are listed in Table 1.

### Modeling the relationship between the elastic properties and porosity

As recalled above, porosity is a fundamental microstructural parameter for the majority of geomaterials that affects

**Table 1** Measured and calculated petrophysical parameters of the studied core samples

Fm.	No.	$\varphi$ (%)	$\rho_b$ (g/cm <sup>3</sup> )	$\rho_g$ (g/cm <sup>3</sup> )	$V_p$ (m/s)	$V_s$ (m/s)	$\mu$ (10 <sup>10</sup> Pa)	$\kappa$ (10 <sup>10</sup> Pa)	$E$ (10 <sup>10</sup> Pa)	$\sigma$
Mdairej Formation	35	2.91	2.63	2.71	6022	3383	3.01	5.52	7.63	0.27
	34	2.58	2.64	2.71	6385	3607	3.43	6.18	8.69	0.27
	33	2.14	2.67	2.73	6112	3513	3.30	5.59	8.27	0.25
	32	4.09	2.63	2.74	5302	3201	2.70	3.80	6.54	0.21
	31	3.89	2.62	2.73	5579	3207	2.70	4.56	6.75	0.25
	30	6.18	2.59	2.76	5073	2942	2.24	3.67	5.58	0.25
	29	5.32	2.59	2.74	5201	3054	2.42	3.79	5.98	0.24
Abeih Formation	28	8.51	2.52	2.75	5367	3050	2.34	4.13	5.91	0.26
	27	8.46	2.52	2.75	5379	3109	2.44	4.04	6.08	0.25
	26	8.28	2.54	2.77	5211	3048	2.36	3.75	5.85	0.24
	25	7.21	2.56	2.76	5240	2879	2.12	4.20	5.44	0.28
	24	2.66	2.62	2.69	5829	3256	2.78	5.21	7.09	0.27
	23	6.51	2.55	2.73	4938	2896	2.14	3.37	5.29	0.24
	22	7.15	2.56	2.76	5548	3189	2.60	4.41	6.52	0.25
	21	7.19	2.58	2.78	5609	3187	2.62	4.62	6.60	0.26
	20	3.24	2.64	2.73	5877	3320	2.91	5.24	7.37	0.27
	19	4.41	2.58	2.69	5843	3339	2.88	4.97	7.23	0.26
Chouf Formation	18	8.52	2.45	2.68	4215	2342	1.34	2.56	3.43	0.28
	17	10.05	2.41	2.68	4181	2362	1.34	2.42	3.40	0.27
	16	6.88	2.51	2.69	4743	2933	2.16	2.77	5.14	0.19
	15	6.35	2.49	2.66	4985	2855	2.03	3.48	5.10	0.26
	14	5.17	2.52	2.66	4843	3027	2.31	2.83	5.45	0.18
	13	9.06	2.46	2.70	4246	25,278	1.57	2.34	3.85	0.23
	12	5.41	2.53	2.67	4985	3040	2.34	3.17	5.63	0.20
	11	4.77	2.54	2.67	4840	2900	2.14	3.10	5.21	0.22
	10	7.76	2.49	2.70	4246	2483	1.54	2.44	3.81	0.24
	9	8.11	2.45	2.66	4085	2401	1.41	2.21	3.49	0.24
8	8.17	2.44	2.65	4386	2611	1.66	2.48	4.08	0.23	
7	5.06	2.51	2.64	4896	2880	2.08	3.24	5.14	0.24	
6	4.51	2.52	2.64	4885	2940	2.18	3.11	5.30	0.22	
5	6.17	2.51	2.67	4476	2758	1.91	2.48	4.56	0.19	
4	7.72	2.46	2.66	4645	2795	1.92	2.75	4.68	0.22	
3	9.11	2.43	2.67	3885	2246	1.23	2.03	3.06	0.25	
2	8.17	2.48	2.70	4586	2730	1.85	2.75	4.53	0.23	
1	7.06	2.46	2.64	4346	2650	1.73	2.34	4.16	0.20	
Minimum		2.14	2.41	2.64	3885	2246	1.23	2.03	3.06	0.18
Maximum		10.05	2.61	2.78	6385	3607	3.43	6.18	8.69	0.28
Average		6.25	2.53	2.70	5028	2933	2.22	3.59	5.51	0.24

Units are as indicated

$\varphi$ , porosity;  $\rho_b$ , bulk density;  $\rho_g$ , grain density;  $V_p$ , primary wave velocity;  $V_s$ , secondary wave velocity;  $\mu$ , shear modulus;  $\kappa$ , bulk modulus;  $E$ , Young's modulus;  $\sigma$ , Poisson's ratio

significantly their elastic and mechanical properties. In order to model this porosity dependency, we apply the GMR (see Ji 2004; Ji et al. 2004, 2006) in this study. We recall below the major characteristics of the GMR for applying it to model the variations of seismic velocities and

elastic moduli as a function of porosity. For a composite made of  $N$  material components, the GMR can be expressed in the following way:

$$M_c^J = \sum_{i=1}^N (v_i M_i^J) \quad (10)$$

where  $M_c$  is a certain property (e.g.,  $V_p$  or Young's modulus) of the composite material,  $N$  is the number of components in the composite,  $i$  is the component index, and  $v_i$  is the component volume fraction given that:

$$\sum_{i=1}^N v_i = 1. \quad (11)$$

The exponent  $J$  in Eq. (10) reflects the effects of microstructures and is controlled essentially by the shape, size distribution, and the distribution of the phases (Ji 2004; Ji et al. 2004). According to Ji et al. (2006), intergranular, continuous, channel pores cavities induce generally a lower  $J$  value than intragranular, isolated, and rounded pores.  $M_c(J)$  has a number of characteristics which are explained in detail in Ji et al. (2006) and Yu et al. (2016) and briefly introduced here. Mathematically, the case of  $J = 0$  is singular but the GMR tends to the geometric average when  $J$  tends to 0. Other cases to be noted are  $J = 1$ , and  $J = -1$  which yield, respectively, the arithmetic average (Voigt) and the harmonic average (Reuss). The exponent  $J$  has values that lie between 0 and 1 for any of the four elastic moduli ( $\mu$ ,  $\kappa$ ,  $E$ , and the Lamé parameter  $\lambda$ ) and can be larger than 1 for seismic velocities (Yu et al. 2016). The microstructural dependent variations of  $J$  produce a wide range of variations in the seismic and elastic properties of solids. Moreover, porosity has a greater effect on the mechanical properties at smaller values of  $J$ .

For the case of a porous material consisting of two-phase components, Eq. (10) reduces to:

$$M_c^J = (1 - p)M_s^J + pM_f^J \quad (12)$$

where  $p$  is the volume fraction of pores,  $M_s^J$  is the property of the solid phase, and  $M_f^J$  is the property of the fluid phase. Porous materials (such as rocks) are a special class of two-phase composites in which pores of a null strength are dispersed within a solid framework. Neglecting the mechanical property of the weak fluid phase, Eq. (12), therefore, leads to:  $M_c^J = (1 - p) M_s^J$ , or equivalently:

$$\frac{M_c}{M_s} = (1 - p)^{\frac{1}{J}} = \left(\frac{\rho_c}{\rho_s}\right)^{\frac{1}{J}} \quad (13)$$

where  $\rho_c$  and  $\rho_s$  are the densities of the porous and non-porous materials, respectively.  $\rho_c/\rho_s$  is a relative density term equivalent to the volume fraction mass.

In the present paper, we apply Eq. (13) to model the variations of seismic velocities and elastic moduli as a function of porosity fitting the cores measurements. We can notice that the relationship is a power relation with respect to the solid volume fraction  $v_s = 1 - p$ . As a consequence,

it is straightforward to apply least squares fitting methods provided by any spreadsheet software considering a power relation. Equivalently, one can use a standard linear least square fitting on the logarithm of  $M_c$ ; i.e., considering the equation:

$$\log(M_c) = \log(M_s) + \frac{1}{J} \log(1 - p) = a + bx. \quad (14)$$

In Eq. (14), the slope of the fitted line is, thus,  $b = 1/J$ .

One can notice that doing so, we neglect the possibility of introducing different uncertainties on each measurement. In other words, we assume that all measurements have the same accuracy or quality. An additional remark is that the range of porosity used for fitting is quite narrow, thus the resolution on the  $J$  exponent is weak and does not allow prediction of the elastic properties for the whole range of porosity.

## Results

### Petrography

The results of the petrographic investigation of the studied rocks are summarized in Table 2. This table includes rock names based on the classifications of Folk (1962) and Dunham (1962), bioclast and non-bioclast components, matrix and cement types, type of porosity, grain shape and packing. Lithology and porosity characterizations under both the SEM and light microscope are illustrated in Figs. 7 and 8. Four rock types (lithofacies) were petrographically identified as briefly explained in the following paragraphs.

### Arenitic sandstone

This rock type was found in samples 4, 7, 11, and 15. The arenitic sandstone is composed mainly of quartz with minor amounts of feldspar and traces of mica in samples 4, 11, and 15, while it is of pure quartz in sample 7 (Fig. 7a–f). Minor constituents of sparite and iron oxide are found between the dominant quartz grains. The grains are angular, elongated, and poorly sorted. This facies exhibits moderate to high porosity, which is of two types. The first is the intergranular pores which are partially filled with precipitates from secondary solutions, thus diminishing the porosity and permeability (Fig. 7e, f). The second porosity type arises from fractures that seem to be very recent and not affected with a secondary dissolution or precipitations (Fig. 7f).

**Table 2** Results of the petrographic investigation of the studied fades

Sample no.	Rock name	Grain ratio		Porosity	Matrix	Cement	Roundness sphericity	Sorting	Grain size and packing
		Bioclast	Non-bioclast						
4	Aranetic sandstone	0%	70% Quartz 10% Feldspar trace, glocunite trace, mica	No porosity	20%	Iron oxide	Angular elongated	2	Matrix supported
7	Aranetic sandstone	0%	100% Quartz	Intergranular and intragranular within the matrix	Iron oxide	Spa rite	Angular elongated	2	Matrix supported
11	Aranetic sandstone	0%	85% Quartz trace, feldspar	Intergranular high porosity	Iron oxide micrite	–	Sub-round elongated	1	Grain supported
15	Aranetic sandstone	0%	90% Quartz trace, feldspar	Intergranular intercrystalline high porosity	Iron oxide micrite	–	Angular elongated	2	Grain supported
19	Lithic limestone	5% Forams sponges plants	60% lithics	Intergranular	5% calcite clay silicate	–	Round elongated	2	Matrix supported
20	Lithic limestone	5% Forams sponges plants	60% lithics	Intergranular	5% calcite	–	Round elongated	2	Matrix supported
22	Oolitic limestone	0%	100% oolite trace, lithoclast	Rare	Clay micrite	Calcite sparite	Angular round	2	Matrix supported
23	Oolitic limestone oosparomicrite	Tr, coral fragments and plants remnants	100% oolite medium preserved	Intergranular	Calcite micrite	Calcite sparite	Round	1	Matrix supported
24	Oolitic limestone oosparomicrite	0%	100% oolite trace, very poor preserved	Intergranular	Calcite and iron oxide micrite	High calcite sparite	Round	2	Sparite supported
25	Oolitic limestone oosparomicrite	3% calc fragments	100% oolite Trace, well preserved	Intergranular and moldic high porosity	20% calcite and iron oxide micrite	–	Round	2	Matrix supported
26	Oolitic limestone oosparomicrite	0%	100% oolite trace, lithoclast well preserved	Intergranular low porosity	Calcite and iron oxide micrite	Calcite sparite	Round	2	Sparite and matrix supported
27	Oolitic limestone oosparomicrite	0%	100% oolite trace, lithoclast well preserved	Intergranular 5% intragranular low porosity	Calcite micrite	Calcite sparite	Round	2	Grain supported
31	Micritic limestone mudstone–wackstone biomicrite	10%, foram skeletons and ostracods	5% fine grains	10% fracture filled with calcite or not moldic, channel	85%	Calcite	–	2	Fine matrix supported
33	Micritic limestone mudstone–wackstone biomicrite	7%, foram and ostracods	5% fine grains	10% fracture filled with calcite or not moldic	93%	Calcite	–	1	Fine matrix supported



### Lithic limestone

This facies is referred to as wackstone–backstone based on Dunham's classification and is detected in samples 19 and 20. A microcrystalline matrix is supporting the majority of lithoclasts (Fig. 7g–k). Traces of foraminifera, sponges, and plant fragments are recognized (Fig. 7h). The poor preservation of the grains and the partial absence of the matrix suggest a highly energetic environment. Two types of porosity were detected in the samples belonging to this facies; the first of which is intergranular porosity diminished partially with the secondary precipitation. Iron oxide cement is filling the pores between the grains (Fig. 7J). The second type of porosity is represented by empty fractures that form a channel-like shape (Fig. 7i, k). These irregular shapes indicate that some solution enlargement occurred differentially along the fractures (Fig. 7i). A secondary precipitation closed some of these pores partially (Fig. 7k).

### Oolitic limestone

This facies is enriched with nonbioclasts and high amount of sparite and micrite (Figs. 7m–t, 8a–h) and is named oosparomicrite based on Folk's classification. Traces of bioclast fragments were observed in sample 25. The micrite consists mainly of calcite and iron oxides, whereas the sparite consists only of calcite. The sparite fills some voids partially between the oolite grains hence diminishing porosity in some parts. Preservation is greatly variable among the samples; for example, sample 25 shows poorly preserved grains (Fig. 7n, p), while sample 26 displays very well-preserved grains (Fig. 8a, b). This observed diversity in grain preservation reflects correspondingly variations in the paleoenvironmental setting. The poorly preserved components might represent the allochthonous grains which have been removed from one system to another. Two types of porosity are detected in the samples of this facies. The first is intergranular porosity which is reduced by secondary precipitation. In sparite-supported samples, the porosity is too low compared with the matrix-supported samples. Moreover, the iron oxide matrix and calcite cement reduced the porosity too. The second type of porosity is represented by microfractures which are rarely detected and which did not significantly enhance the porosity (Fig. 8e, f).

### Micritic limestone

This facies is referred to as mudstone–wackstone based on Dunham's classification or fossiliferous biomicrite based on Folk's classification. This type of rock is encountered, for example, in sample 31. In these rocks, the microcrystalline texture appears in Fig. 8i, j with 5–10% of bioclasts

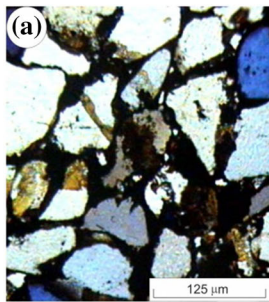
and non-bioclasts including lithic clasts (Fig. 8i–t), planktonic/benthonic foraminifera (Fig. 8n) and ostracods (Fig. 8p). The preservation is good in the investigated specimens suggesting an oligotrophic environment for the water column. The low percentage of bioclasts and non-bioclasts is associated with matrix-supported very poorly sorted grains. Three types of porosity were detected in these samples: (1) intergranular and intragranular porosity with a very few percentage of moldic porosity. The later was found inside the bioclast grains, mainly in the foraminifera, ostracods, and bone fragments (Fig. 8n, p–r, t). Some bioclasts are filled with secondary precipitation (Fig. 8s). Micropores between the grains were also observed (Fig. 8m, q); (2) fractures filled with calcite were observed in the studied samples mainly in two ways; first, the fractures are occasionally filled with the secondary calcite while others are fully filled with secondary precipitation (Fig. 8q, s); and (3) empty fractures forming a channel-like shape (Fig. 8s). These irregular shapes indicate that some solution enlargement occurred along the fractures (Fig. 8t).

### X-ray diffraction analysis

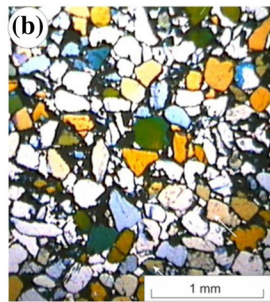
The results of the XRD analysis (Fig. 9) reveal that the investigated rocks can be divided into two main categories: limestones and sandstones (i.e., carbonates vs. clastics). Calcite is the essential carbonate mineral component of samples 20, 26, and 31 (Fig. 9a). Minor minerals including clays, plagioclase, and quartz are also recognized in some samples. The presence of minor amounts of quartz in the limestones suggests that siliceous deposits have precipitated during diagenesis where they partially filled the pore spaces. In the sandstones, quartz is the dominant mineral (Fig. 9b); reaching 94%, for example, in sample 4 (Fig. 7a–f). Minor amounts of clay minerals and calcite are also identified. Calcite might have precipitated by migrating solutions during the diagenesis in the arenitic sandstone facies where it fills partially the pores and thus reducing the rock porosity.

### Petrophysical characteristics

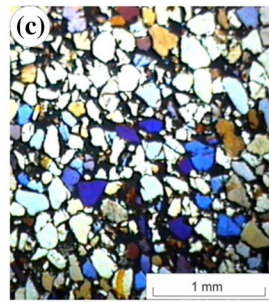
Porosity of the studied samples is generally low and varies from 2.14 to 10.05% with an average of 6.25% (Table 1). These poor porosity values are confirmed by the petrographic study of the four microfacies (Table 2) where the porosity is very low in the micritic limestones and in the mud-supported lithologies (Fig. 8), or where the secondary precipitations and filling of the primary porosity took place (Fig. 7). The SEM images also reveal small volumes of many pores and thus poor porosity (Figs. 7, 8). The low porosity may also result from the presence of pore-filling



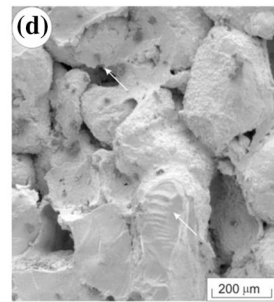
Sample 4, Arenitic Sandstone



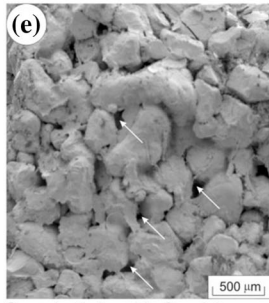
Sample 4, Arenitic Sandstone



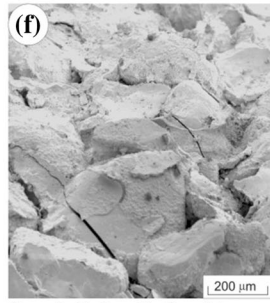
Sample 4, Arenitic Sandstone



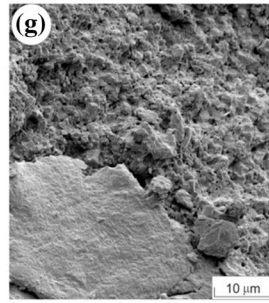
Sample 7, Arenitic Sandstone



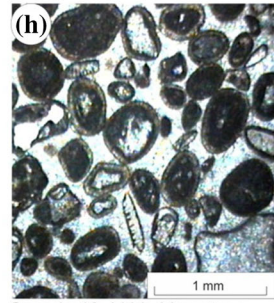
Sample 7, Arenitic Sandstone



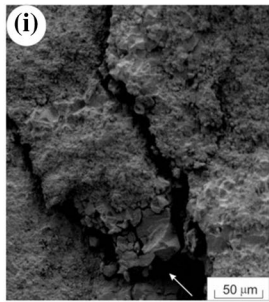
Sample 7, Arenitic Sandstone



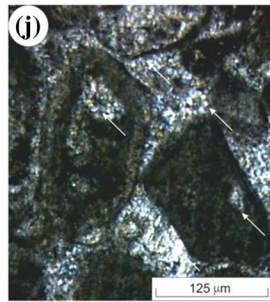
Sample 19, Lithic Limestone



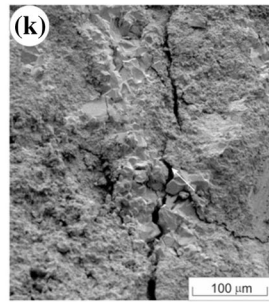
Sample 19, Lithic Limestone



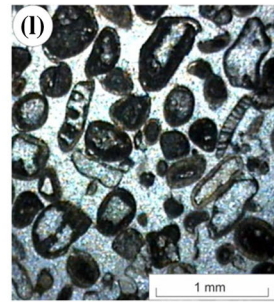
Sample 19, Lithic Limestone



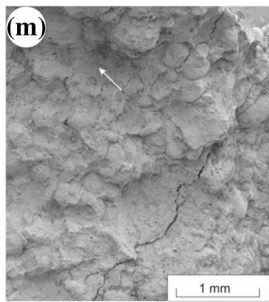
Sample 19, Lithic Limestone



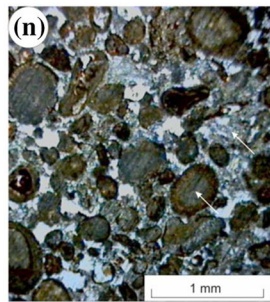
Sample 19, Lithic Limestone



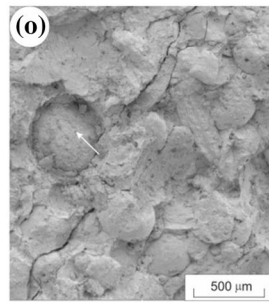
Sample 19, Lithic Limestone



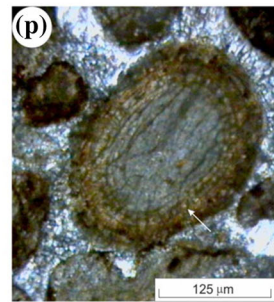
Sample 25, Oolitic Limestone



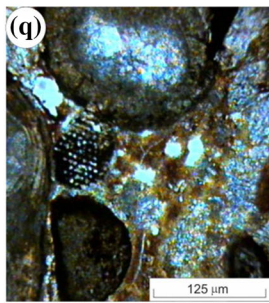
Sample 25, Oolitic Limestone



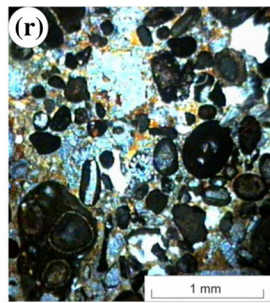
Sample 25, Oolitic Limestone



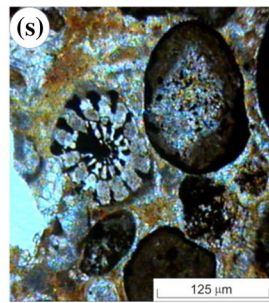
Sample 25, Oolitic Limestone



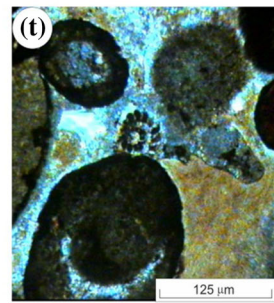
Sample 25, Oolitic Limestone



Sample 25, Oolitic Limestone



Sample 25, Oolitic Limestone



Sample 25, Oolitic Limestone



◀ **Fig. 7** Transmitted light and SEM microphotographs from the Lower Cretaceous Chouf and Abeih Formations exposed at central Lebanon. Arenitic sandstone facies of the Chouf Formation (a–c) with minors of sparite and iron oxide matrix between the grains. Some intergranular pores (d, e) are filled partially with cement materials deposited by secondary solutions. Microfractures (f) are formed which may slightly enhance the porosity. g–l Lithic limestone of the Abeih Formation showing the microcrystalline matrix supporting the majority of lithoclasts with secondary fractures (i, k) and iron oxide cement (j) between the lithic grains. m–t The oolitic limestone facies of the Abeih Formation with fracture porosity (m, o) and fossil remains (q, s, t)

materials represented by carbonates, and iron oxides; a common feature that was observed also at other rocks from different formations (e.g., Mousa et al. 2011). Based on these low porosity data, bulk density values are moderate to high (higher than  $2.41 \text{ g/cm}^3$  for all samples) which might be induced by intensive compaction and cementation as shown in the oosparomicrite and micritic limestone textures. The observed bulk density values vary narrowly from 2.41 to  $2.67 \text{ g/cm}^3$  with an average of  $2.53 \text{ g/cm}^3$ . The lowest bulk densities are encountered in the clastic facies of the Chouf and the base of Abeih Formations, whereas the highest are recorded for the upper part of the Abeih Formation and the compact limestones of the Mdairej Formation (Table 1). The grain density varies slightly from 2.64 to  $2.78 \text{ g/cm}^3$  with an average of  $2.70 \text{ g/cm}^3$ .

The measured  $V_p$  varies widely between 3885 and 6385 m/s with an average value of 5028 m/s for the studied rock samples. The  $V_s$  values, on the other hand, vary between 2246 and 3607 m/s, with an average of 2933 m/s. The calculated  $V_p$  and  $V_s$  averages give a slightly low  $V_p/V_s$  ratio of 1.71, consistent with an average Poisson's ratio of 0.24 (Table 1). The average values of the shear, bulk, and Young's moduli, as calculated from the measured acoustic wave velocities and the bulk density, are  $2.22 \times 10^{10} \text{ Pa}$ ,  $3.59 \times 10^{10} \text{ Pa}$  and  $5.51 \times 10^{10} \text{ Pa}$ , respectively. In the following paragraphs, we investigate how these petrophysical parameters are related to each other and the way in which the composition and the depositional history of the studied rocks impacted these significant rock characteristics.

### Porosity versus bulk density

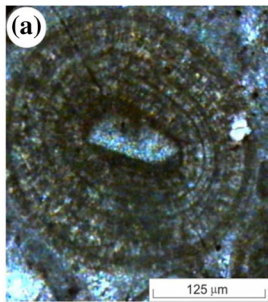
Porosity and bulk density are major parameters influencing the physical and mechanical properties of many sedimentary rocks (e.g., Abu Seif 2016), and are usually very closely related. The relationship between these two parameters is routinely investigated to check the reliability of the measured data. While the grain density is a good

indicator of the mineral composition, the bulk density reflects the combination between mineral composition and porosity (Nabawy and Barakat 2017). The relationship between porosity and bulk density is shown in Fig. 10a, where the two parameters are inversely correlated to each other, showing a porosity-dependent decreasing function of bulk density. This trend fits the general form of the porosity–density relation confirmed by many other researchers (e.g., Han and Batzle 2004). If the relation is strongly linear, this means that the grain density data are similar which characterizes homogenous lithologies (Nabawy et al. 2015; Nabawy and David 2016). The observed scatter in this relationship (Fig. 10a) is, therefore, related to lithological variations.

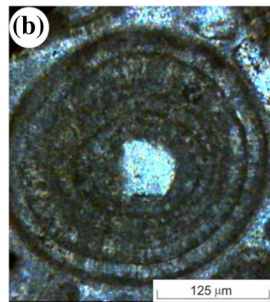
Similar to the clastic facies of the Chouf Formation, the base of the Abeih Formation is also dominated by clastic rocks while the remaining part of it and the overlying Mdairej Formation are composed mainly of carbonates (Fig. 2). Therefore, we merge the samples of the Chouf Formation and the two lowermost samples collected from the Abeih Formation (i.e., samples 1–18 in Table 1 and Fig. 2) into one group and identify it as the clastic facies (group I), whereas the remaining samples from Abeih and those of Mdairej Formations (i.e., samples 19–35 in Table 1 and Fig. 2) represent the carbonate facies (group II). In Fig. 10b we construct the relationship between porosity and bulk density for the clastic and carbonate facies separately. Although carbonates display generally a wide scatter with low correlation coefficients (Kassab et al. 2016) as being more sensitive to diagenetic alterations, group II samples of the carbonate facies exhibit a less scatter with a higher  $R^2$  value of 0.9. Group I samples, on the other hand, show a wider scatter and a weaker correlation coefficient ( $R^2 = 0.84$ ; Fig. 10b) probably because of a higher clay content. Nonetheless, these relationships with their high correlation coefficients indicate that porosity can be predicted from the simply calculated bulk density data of these rocks with a high precision.

### Porosity versus grain density

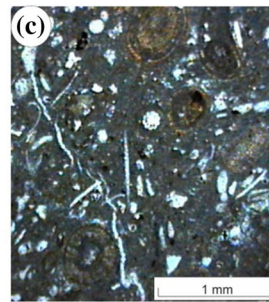
The relationship between grain density and porosity displays a very wide scatter to the degree that it is too difficult to infer any clear trend (Fig. 10c). This indicates the weak lithology-dependent porosity of the studied samples and that depositional conditions and diagenetic alterations are more effective on porosity rather than the original composition of the rocks. However, constructing the relationship between the two parameters for the two groups of samples displays a good separation between the clastics having lower grain densities (average  $2.66 \text{ g/cm}^3$ ) and slightly higher porosities from the carbonates with their



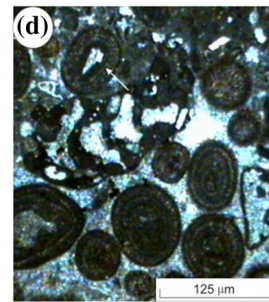
Sample 26, Oolitic Limestone



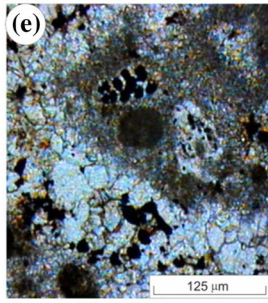
Sample 26, Oolitic Limestone



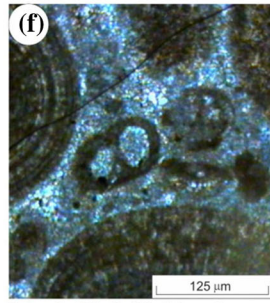
Sample 26, Oolitic Limestone



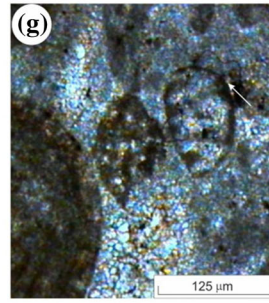
Sample 26, Oolitic Limestone



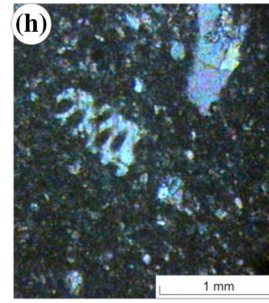
Sample 26, Oolitic Limestone



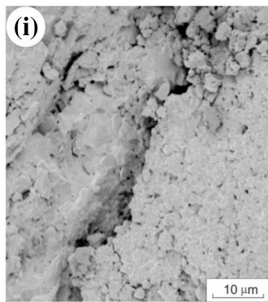
Sample 26, Oolitic Limestone



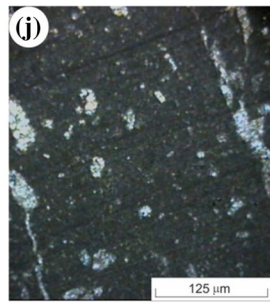
Sample 26, Oolitic Limestone



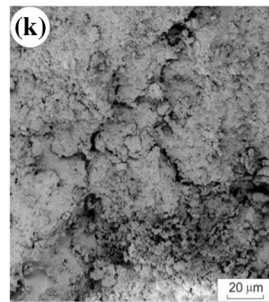
Sample 26, Oolitic Limestone



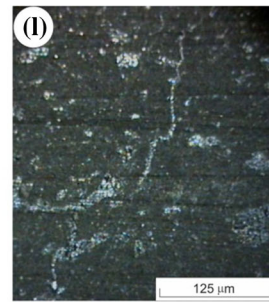
Sample 31, Micritic Limestone



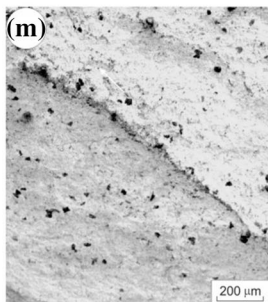
Sample 31, Micritic Limestone



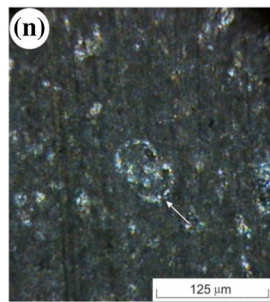
Sample 31, Micritic Limestone



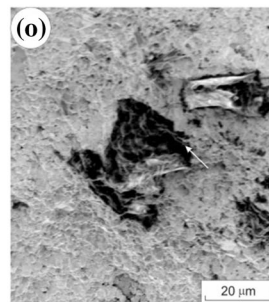
Sample 31, Micritic Limestone



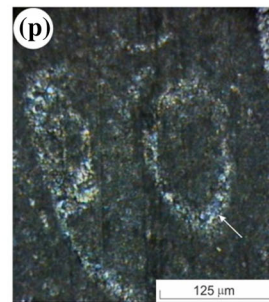
Sample 31, Micritic Limestone



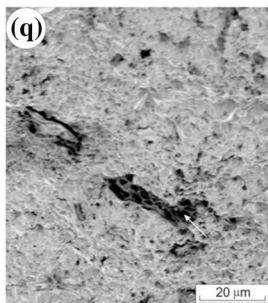
Sample 31, Micritic Limestone



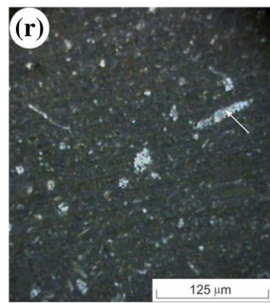
Sample 31, Micritic Limestone



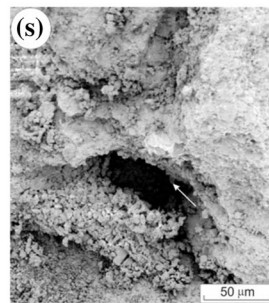
Sample 31, Micritic Limestone



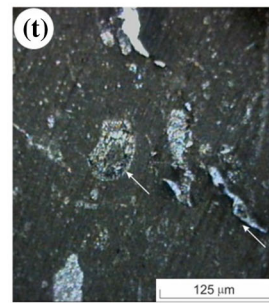
Sample 31, Micritic Limestone



Sample 31, Micritic Limestone



Sample 31, Micritic Limestone



Sample 31, Micritic Limestone



◀ **Fig. 8** Transmitted light and SEM microphotographs from the Abeih and Mdairej Formations. **a–h** Oolitic limestone of the Abeih Formation with well-preserved oolitic grains (**a, b**), iron oxide matrix-supported grains (**c, h**) and sparite-supported grains (**d–g**). **i–t** The micritic limestone of Mdairej Formation with intergranular and intragranular porosity (**i, o**), secondary fractures (**k**) and fossil remains (**n, p, t**)

relatively higher grain densities (average  $2.74 \text{ g/cm}^3$ ) and variable porosity (Fig. 10d).

### Porosity versus seismic wave velocities

Seismic wave velocity is strongly porosity dependent (e.g., Rafavich et al. 1984; Wang and Nur 1992; Wang et al.

2009). A plot of velocity versus porosity displays generally an inverse trend where velocities decrease with the increase of porosity. For laboratory experiments on a wide variety of rocks, Castagna et al. (1985) observed a decrease of both  $V_p$  and  $V_s$  with the increase of porosity. Therefore, an increase in porosity is always accompanied by a corresponding decrease in velocity simply because seismic velocity in the pores is lower than that in the grains constituting the rock. Figure 11a, b displays the inverse relationships between porosity and both  $V_p$  and  $V_s$  for the studied samples. In general, both  $V_p$  and  $V_s$  decrease with increasing  $\phi$ , but with a wide scatter and fair  $R^2$  (0.51–0.69) values. The obtained  $J(V_p)$  and  $J(V_s)$  values, upon applying the GMR, are relatively low (vary from

**Fig. 9** Results of the XRD analysis of selected samples with the abundance of **a** carbonate minerals and **b** quartz. Minor amounts of clays are also present

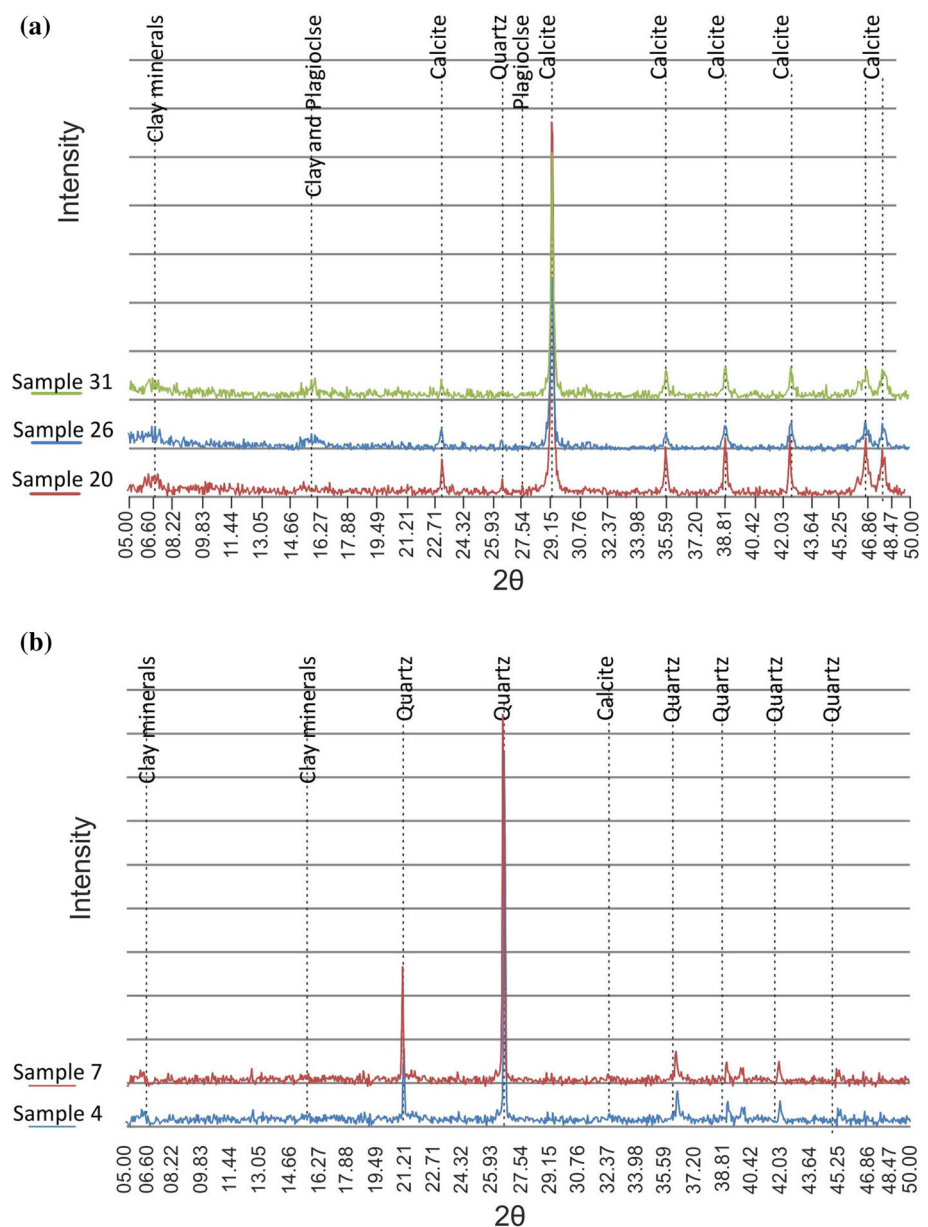
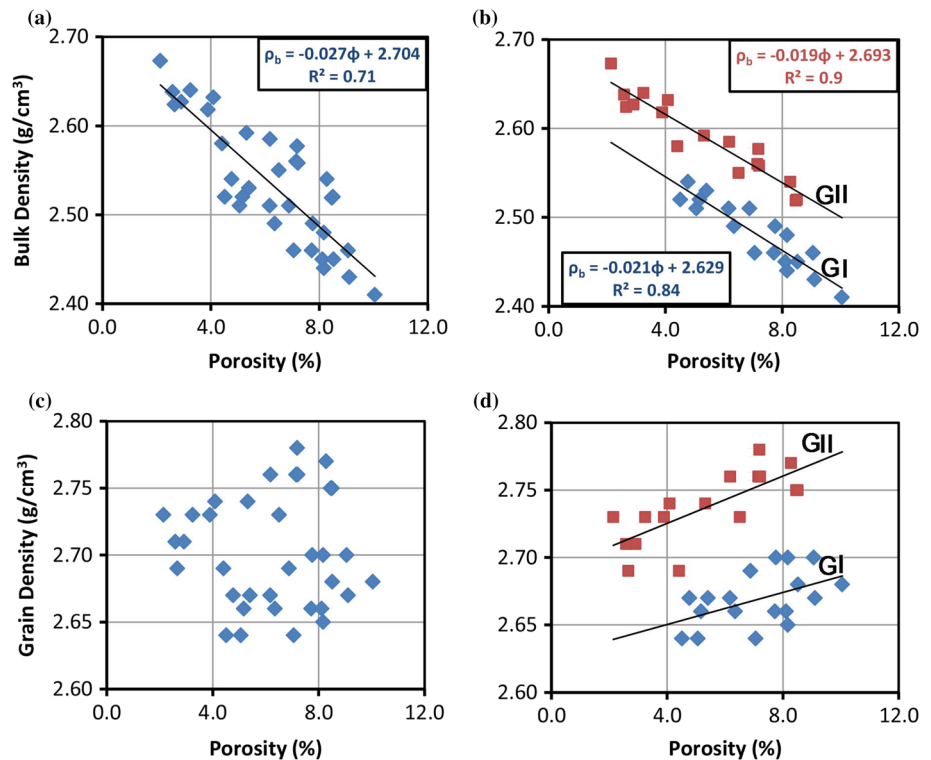


**Fig. 10** Interrelationships between porosity versus bulk (a, b), and grain (c, d) densities. The blue rhombs denote group I (GI) samples, whereas the red squares denote the samples of group II (GII; see text for more details)



0.221 to 0.499), implying a stronger effect of porosity on the observed seismic wave velocities (Yu et al. 2016).

The wider scatter encountered in the carbonate facies may be induced by the generally higher sensitivity of the carbonates to the dissolution, cementation, and diagenetic processes compared to the clastic rocks. Different types of pore spaces, pore geometry, and variable composition induced partly by the depositional conditions, and modified later by the diagenetic processes (Figs. 7, 8) may be responsible for the high scatter observed in the carbonates. These observations are consistent with the nonlinear dependence of seismic wave velocities on porosity which has been observed by other researchers (e.g., Wyllie et al. 1956; Schön 1996; Anselmetti and Eberli 1999; Arns et al. 2002; Eberli et al. 2004; Knackstedt et al. 2005; Baechle et al. 2008; Weger et al. 2009; Fabricius et al. 2010; Kassab and Weller 2011). On the other hand, other researchers including, for example, Han et al. (1986); Knackstedt et al. (2003); and Wang et al. (2009) observed a linear relationship between porosity and seismic wave velocity in clastic rocks.

### Porosity versus elastic moduli

The elastic constants reported in Table 1 are calculated from the measured seismic wave velocities and the bulk density of the studied rocks. Because the seismic wave velocities are themselves dependent on porosity, we expect

that the elastic moduli will also be porosity dependent. The relationships between porosity and the three elastic moduli ( $\mu$ ,  $\kappa$ , and  $E$ ) are shown, respectively, in Fig. 11c–e, where clear inverse trends are observed. These inverse trends confirm the porosity-dependent elastic properties of rocks. In addition, the obtained  $J(\mu)$  and  $J(E)$  values are low compared to those reported in the study of Yu et al. (2016), which again implies a stronger porosity dependency of the elastic properties of the studied rocks. The variable lithology and the consequent complex nature of the pore system of the studied rocks may explain the considerable scattering which results in fair/moderate correlation coefficients (Fig. 11c–e). It is noticed that group II samples of the carbonate facies show a wide scatter due to the variability of their porosity and strong impact of the diagenetic processes on carbonates.

The relationship between porosity and  $\sigma$  shows no clear trend (Fig. 12a); although the carbonate samples show a tendency of having higher Poisson's ratio and lower porosities (Fig. 12b) compared with the clastic rocks. Moreover, weakly negative trend is revealed by the carbonate samples, while the clastic rocks display a weakly positive trend. It is well known that the quartz content has a strong effect on  $\sigma$  to the degree that a rock enriched in this mineral or any of its polymorphs may have a negative or very low Poisson's ratio (McSkimin et al. 1965; Ji et al. 2018). Carbonates, on the other hand, have higher  $\sigma$  values which may be up to 0.33 (e.g., Ji et al. 2018). In our

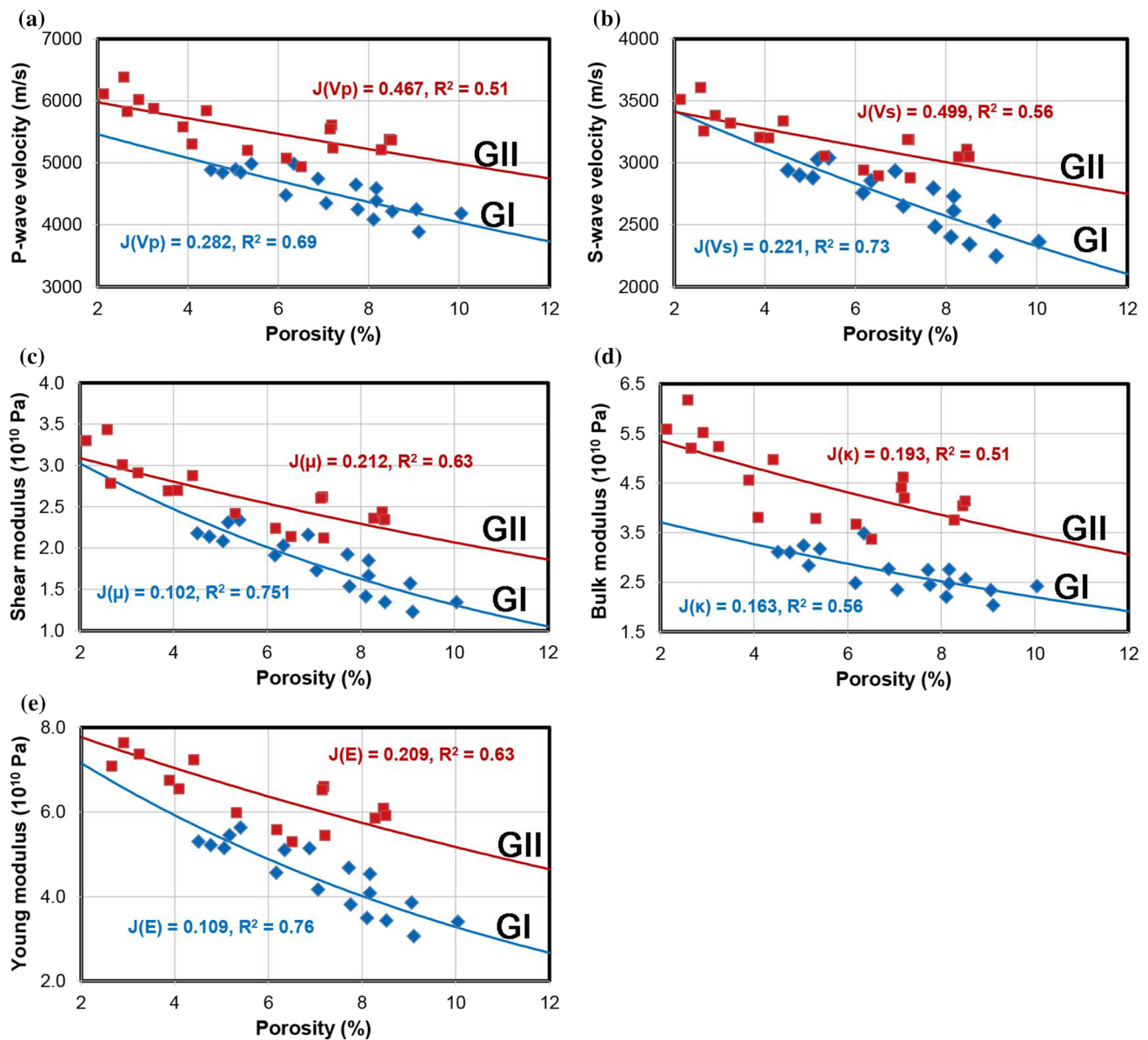


**Fig. 11** Interrelationships between porosity and the seismic wave velocities (a, b) as well as the three elastic moduli,  $\mu$ ,  $\kappa$ , and  $E$  (c–e). Other details are similar to those of Fig. 10

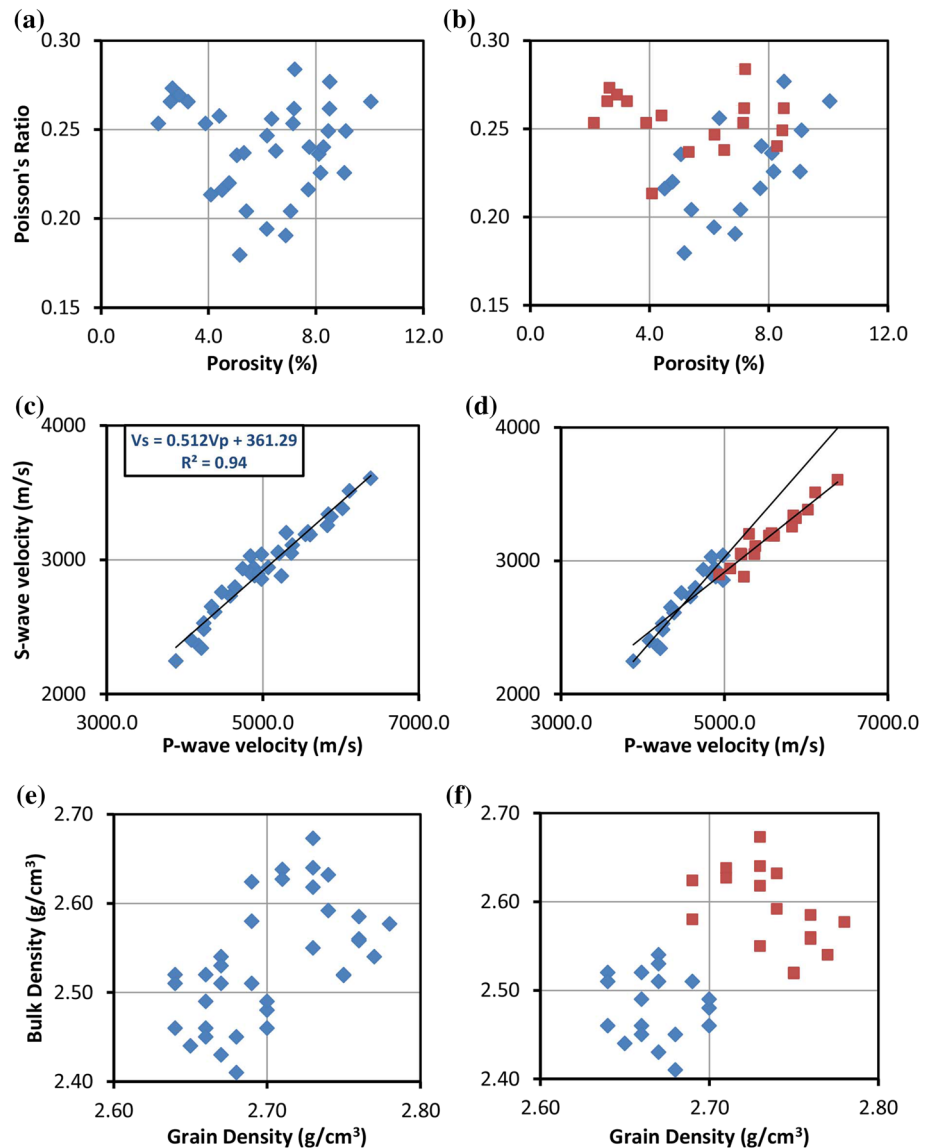
analysis, the highest  $\sigma$  values are observed for the samples of the carbonate group (Fig. 12b, Table 1).

### Compressional wave velocity versus shear wave velocity

The relationship between  $V_p$  and  $V_s$  is shown in Fig. 12c, where they are linearly correlated with a high correlation coefficient ( $R^2 = 0.94$ ), revealing that  $V_s$  can be precisely predicted from the easily, and more commonly, measured  $V_p$ . Such linear relationship between  $V_p$  and  $V_s$  is well established by many other researchers (e.g., Wang et al. 2009). Few samples deviate slightly from the normal, very

concise, trend which may result from variations in sediment properties (Ojha and Sain 2014). Group II samples have higher seismic wave velocities relative to those of group I (Fig. 12d) because of the more compact nature and higher bulk density of carbonate rocks. The slight clockwise rotation of the best fitting line for group II samples caused by the relatively lower  $V_s$  values explains the observed higher  $\sigma$  of the carbonates relative to the clastic facies (see also Fig. 12b, Table 1).

**Fig. 12** Interrelationships between porosity and Poisson's ratio (a, b),  $V_p$  and  $V_s$  (c, d), and between bulk density and grain density (e, f). Other details are similar to those of Fig. 10



### Bulk density versus grain density

The grain density is a good indicator of lithology and, therefore, is used to distinguish carbonates from clastics. Pure clastics usually possess a lower than  $2.65 \text{ g/cm}^3$  grain density, whereas carbonates are characterized by higher than  $2.76 \text{ g/cm}^3$  grain density (e.g., Nabawy et al. 2015). The presence of iron oxide or calcareous cements, however, increases the grain density of the clastic rocks (Nabawy and Barakat 2017). The bulk density, on the other hand, is an indicator of both the pore volume and mineralogical composition. Although a clear positive trend can be observed for all samples (Fig. 12e); a wide scatter is obtained. Few carbonate samples have unexpectedly low bulk densities similar to sandstones (Fig. 12f). These low bulk density values could be induced by impurities in the studied carbonate facies with a significant clastic

proportion rather than large volume of secondary pores formed by dissolution and leaching because the measured porosities for the carbonate samples are generally poor (average 5.34%). The discrimination between the two facies is, however, clear where the clastic group possesses generally lower density values relative to the carbonates. The high correlation coefficient of the relationship between porosity and bulk density for the carbonate facies (Fig. 10a, b) may point to uniform distribution of the effective interstitial pore spaces and homogeneous pore throat size distribution (Nabawy et al. 2015). The presence of bio-components such as foraminifera, ammonites and ostracods supports the idea of uniformity of distribution of the effective interstitial pore spaces within the limestone facies. Particularly, distribution of foraminifera leading to a homogeneous pore throat size distribution can be observed in the micritic limestones.



### Bulk density versus seismic wave velocities and Poisson's ratio

The relationships between bulk density and both  $V_p$  and  $V_s$  data for all samples are illustrated in Fig. 13a, c, where direct trends with moderate correlation coefficients ( $R^2 = 0.82$  for both relationships) are seen. Moreover, and in agreement with the lithologic characteristics of the studied facies, Group II samples are characterized by relatively higher seismic wave velocities and bulk densities compared to the samples of group I (Fig. 13b, d). The plot of bulk density versus  $\sigma$  (Fig. 13e, f) discriminates very well between the clastics (having lower  $\rho_b$  and  $\sigma$ ) from the carbonates with their higher  $\rho_b$  and  $\sigma$  values.

### Grain density versus seismic wave velocities and the Poisson's ratio

Grain density is a diagnostic property of lithology and its relationship with seismic wave velocities and the Poisson's ratio displays direct trends with some scatter (Fig. 14a, c, e). Indeed, the carbonates with their higher seismic wave velocities and higher Poisson's ratio are clearly discriminated from the clastic facies having lower grain densities and slower velocities (Fig. 14b, d, f).

**Fig. 13** Interrelationships between bulk density seismic wave velocities (a–d), and between bulk density and Poisson's ratio (e, f). Other details are similar to those of Fig. 10

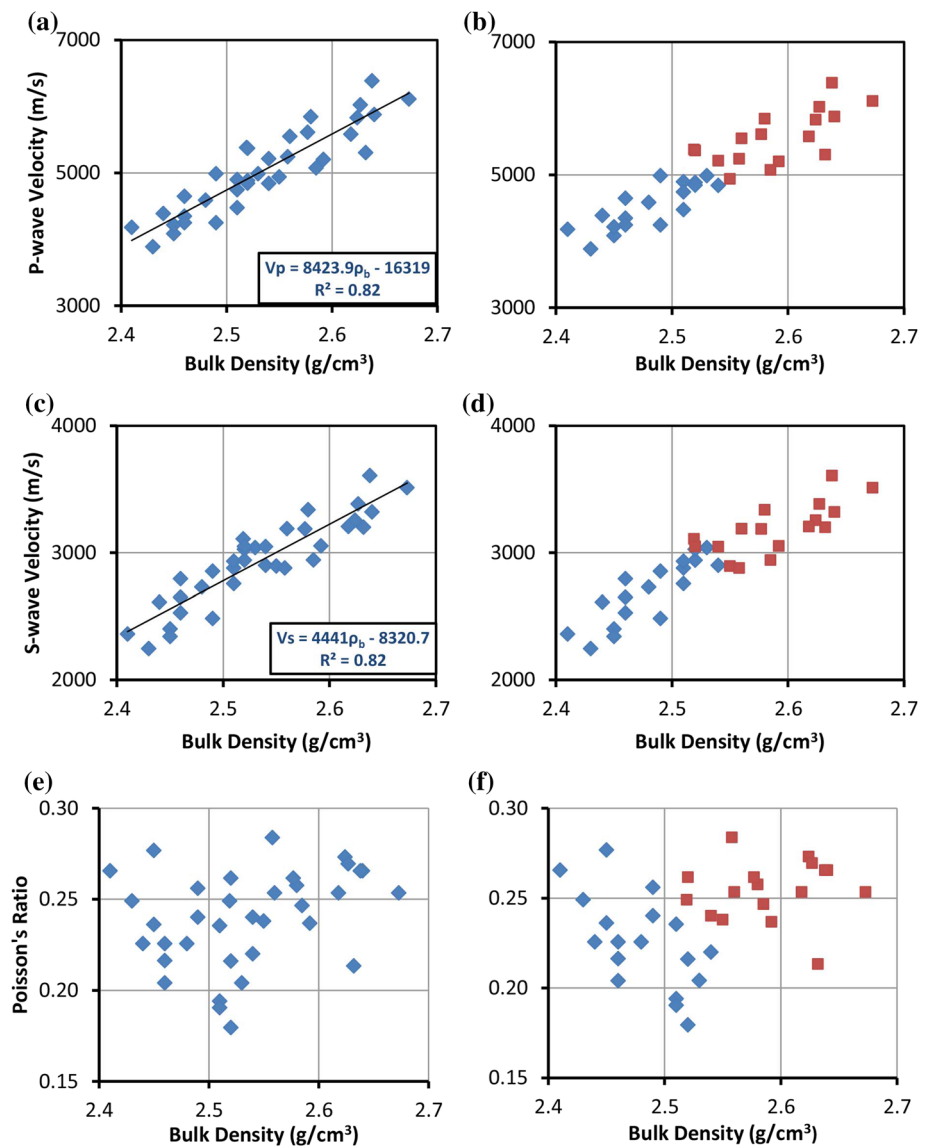
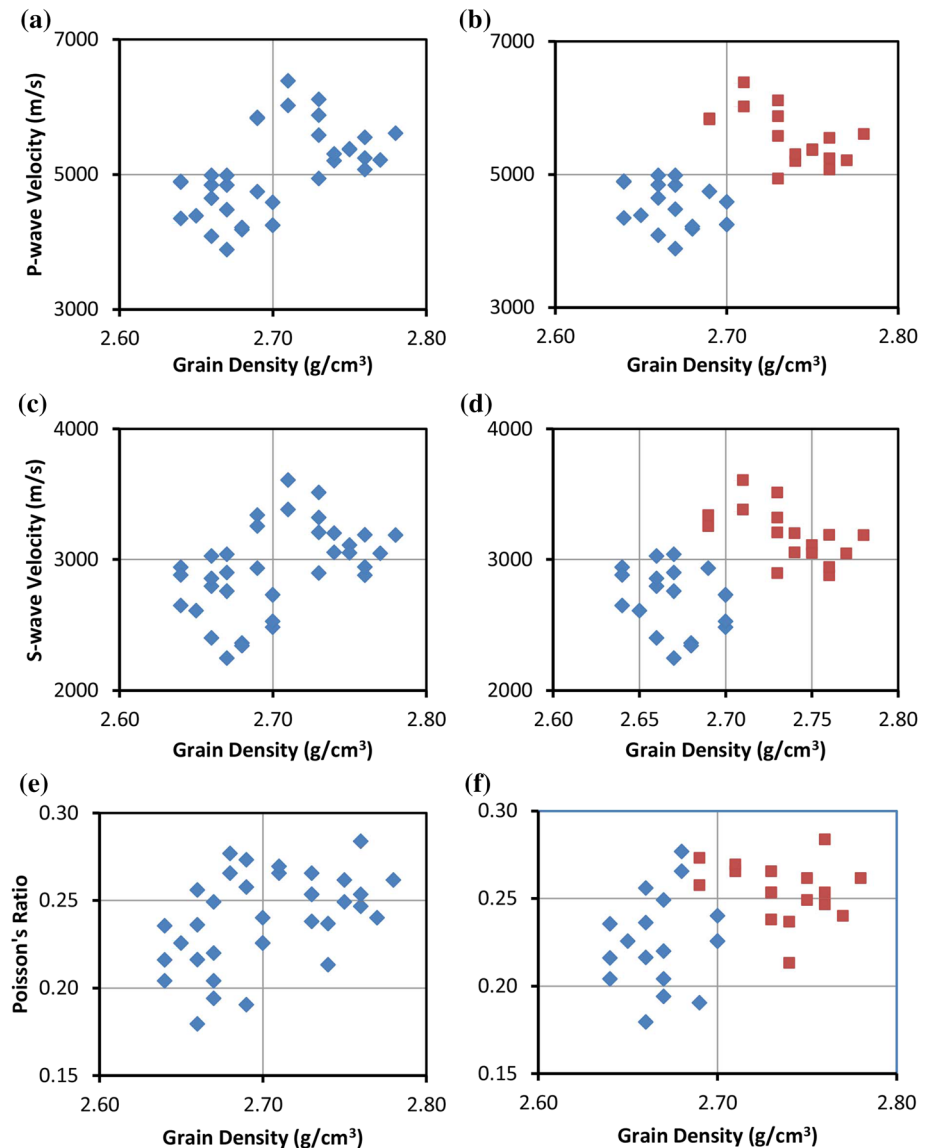


**Fig. 14** Interrelationships between grain density and seismic wave velocities (a–d), and between the grain density and the Poisson's ratio (e, f). Other details are similar to those of Fig. 10



## Discussion

### Porosity and seismic wave velocities

Lithological characteristics comprising the mineral composition, grain packing and contacts, porosity and bulk density, have significant effects on the physical and mechanical properties of sedimentary rocks (e.g., Bell 1978; Shakoor and Bonelli 1991; Ulusay et al. 1994; Dvorkin and Nur 1998; Jeng et al. 2004). Numerous studies have been specifically conducted on the relationships between porosity, bulk density and seismic wave velocities in various regions in the world (e.g., Wyllie et al. 1956, 1958; Gardner et al. 1974; Raymer et al. 1980; Castagna et al. 1985; Hyndman et al. 1993; Erickson and Jarrad 1998; Ojha and Sain 2014). Most of the

interrelationships between these parameters are characterized by moderate correlation coefficients. However, each of these studies focuses only on specific lithology such as siliciclastics or carbonates from specific study areas. For example, Ojha and Sain (2014) found  $R^2$  values between  $V_p$  and  $\varphi$ ; and between  $V_s$  and  $\varphi$ , for carbonate-rich sediments, at 0.77 and 0.73, respectively. Carbonate rocks exhibit less predictable velocity–porosity relationships than those found in siliciclastics because of the complex and heterogeneous pore structures they have (Bashah and Pierson 2012). The complexity of pore spaces is, in turn, related to the rock type and the effect of diagenetic processes (Tucker and Wright 1990). The observed large scattering results in large uncertainties in seismic inversion and calculations from porosity. According to Bashah and Pierson (2012), four main factors, namely pore size, pore system tortuosity, pore circularity, and the percentage of microporosity are

the cause of scattering in the velocity–porosity relationship for carbonate rocks. The high diagenetic potential of carbonates alters the pore structure which is responsible for the observed scattering (Baechle et al. 2004). The equation of Wyllie et al. (1958), which was developed initially for siliciclastics, was later applied also to carbonates and the main inference was that the existing pore types, pore sizes, and the internal geometry of rocks have a great effect on the velocity–porosity relationship and the overall acoustic behavior of carbonates. The presently used GMR is a simple but rigorous mathematical expression providing a unified description of the best fitting relationship between porosity and the overall elastic properties of the studied rocks (Fig. 11).

Previously, Han et al. (1986) investigated the effects of porosity and clay content on the acoustic properties of sandstones and unconsolidated sediments. Although a significant scatter was also revealed, Han et al. (1986) found clear trends indicating that both  $V_p$  and  $V_s$  decrease with increasing porosity. The observed scatter was interpreted to be induced mainly by the clay content. For this reason, some researchers use certain isotropic, man-made, synthetic, materials with well-known porosities to deeply understand the porosity dependence of the seismic properties of natural rocks. In addition, natural rocks may also contain thin disk-shaped microcracks, foliation-parallel cracks, grain boundary cracks, or oblique cracks (e.g., Sun et al. 2012), which may influence the relationship between porosity and the seismic wave velocities and the Poisson's ratio.

### Porosity and the $V_p/V_s$ ratio

Results of Han et al. (1986) revealed that samples with high porosity and clay content tend to have high  $V_p/V_s$  ratios. Porosity values estimated for our samples are generally low which are consistent with the average low  $V_p/V_s$  ratio of 1.68 for the clastic facies. A weakly positive trend was observed between the  $V_p/V_s$  ratio and the porosity of sandstone and silty shale samples collected from a deep hole penetrating the Chelungpu fault in central Taiwan (Wang et al. 2009). In addition, it was noticed that  $V_p/V_s$  increases with increasing porosity in periclase aggregates, sintered porcelain, quartz sandstones, and porous  $\text{SiO}_2$  glasses (Soga and Schreiber 1968; Boisson et al. 1976; Han et al. 1986; Adachi and Sakka 1990). On the other hand, other investigators, including Porter et al. (1977), Panakkal et al. (1990), Berge et al. (1995), Asmani et al. (2001), Yeheskel et al. (2001), and Yu et al. (2016), observed inverse relationships between porosity and Poisson's (or the  $V_p/V_s$ ) ratio for spinel aggregates, silver compacts, iron compacts, alumina ( $\text{Al}_2\text{O}_3$ ) ceramics, and fused glass beads, respectively. These different patterns have been

interpreted to result mainly from different pore aspect (width/length) ratios (Dunn and Ledbetter 1995).

In our study, we can see a direct relationship between porosity and  $\sigma$  for the clastic facies, but a weak inverse relationship for the carbonates (Fig. 12b). Some carbonate rocks possess moderate porosity as a consequence of dissolution and leaching of some components, and therefore are characterized by higher Poisson's ratios (Table 1). Higher  $V_p/V_s$  (and higher  $\sigma$ ) ratios have also been reported for carbonates by previous researchers relative to sandstones. Winkler and Murphy (1995), for example, found  $V_p/V_s$  values of more than 1.8 for limestones and dolomites and values of 1.6–1.7 for clean sandstones. An even lower  $V_p/V_s$  ratio [ $(2)^{1/2} \leq V_p/V_s \leq (3)^{1/2}$ ] is common for some minerals including quartz (Yu et al. 2016). Moreover, sandstones and quartzites have lower Poisson's ratio compared to limestones and marble. In our study, the average  $\sigma$  for the clastic and carbonate groups are 0.23 and 0.25, respectively, and that of the  $V_p/V_s$  ratio are 1.68 and 1.74, respectively. These results are consistent, therefore, with previous observations. However, the relatively low  $V_p/V_s$  value of the carbonate facies in our study relative to the value of 1.8 reported by Winkler and Murphy (1995) might be induced by different measuring pressure conditions or by the impure nature and the small clastic fraction of most of the studied carbonate rocks. In general, information listed in Table 1 and the relationships expressing the elastic properties of the studied facies (Figs. 11a–e, 12b, d, 13b, d, f, 14b, d, f) are in good agreement with previous results.

### Effects of clay and confining pressure

Actual sedimentary rocks such as sandstones and limestones (composed mainly of quartz and calcite, respectively) are rarely clean and often contain other minerals such as clays, iron oxides, evaporites, and feldspars. The petrographic and XRD analyses showed that most of the studied samples contain various quantities of clay minerals (Fig. 9). These minerals have a great effect on the elastic properties of the rocks (Knackstedt et al. 2005). The prevalent conditions at the times of deposition, compaction, bioturbation, and diagenesis affect the amount and distribution manner of the clays within the rock framework. Many existing empirical studies (e.g., Castagna et al. 1985; Han et al. 1986) and theoretical models (Xu and White 1995) account on the volume of clays but ignore their distribution. Han and Batzle (2004) noticed that an increasing clay content decreases the grain bulk and shear moduli. Knackstedt et al. (2005) used computer simulations to calculate the elastic properties of model-cemented sandstones composed of two or more mineral phases. Unlike experimental data, they found that numerical data

exhibit little noise and less scatter even though they cover a wide range of quartz/cement ratios and porosities. In general, their results are in good agreement with the experimental data of clay-bearing consolidated sandstones over a wide range of porosities. Moreover, the estimated modulus–porosity relationships show little dependence on microstructure which is consistent with the previously proposed models that ignore the distribution mode of the clay phase. Presence of clay minerals, most probably kaolinite based on the X-ray charts, in our samples diminished the porosity of the samples as kaolinite crystals occur in blocky forms and within minor pore spaces. Moreover, Kaolinite forms in acidic environments and remains stable (Selley and Sonnenberg 2015), thus giving it a privilege to stay in the pore spaces and diminish the porosity.

Another significant parameter which greatly affects the seismic wave velocity and the elastic behavior of rocks is the confining pressure. The velocity–pressure curves obtained by Ji et al. (2007) are best explained by a four-parameter theoretical exponential equation:  $V(P) = V_0 + DP - B_0 \exp(-kP)$ , where  $V_0$  is the projected velocity at zero pressure if cracks/pores are absent;  $D$  is the intrinsic pressure derivative of velocity in the linear elastic regime;  $B_0$  is the initial velocity drop induced by the existence of cracks/pores at zero pressure; and  $k$  is the decay constant of the velocity drop in the nonlinear poro-elastic regime. Moreover, Ji et al. (2007) detected also a seismic hysteresis which was interpreted as being caused by irreversible changes in grain contacts, increases in the aspect ratio of microcracks, and shrinkage of void space in the pressurization–depressurization cycle. Although still poorly understood, it is well known that seismic hysteresis (different seismic wave velocities during pressurization/depressurization) exists and that seismic velocities during depressurization are higher than those measured during pressurization (Birch 1960; Burke and Fountain 1990). However, we have carried out our velocity measurements under ambient pressure conditions because the investigated rocks are collected from exposed outcrops.

Although we found high correlation coefficients between some petrophysical properties such as that relating the bulk density–porosity and compressional–shear wave velocities ( $R^2 = 0.9$  and  $0.94$ , respectively), many other relationships, unexpectedly, exhibit fair/moderate correlations which could be induced mainly by the variations in the nature of the rock and its diagenetic history. This clearly demonstrates the effects of lithology, the depositional processes, and the subsequent geological conditions on the different petrophysical aspects of the rock. Based on comprehensive analysis of the relationship between porosity and  $V_p$  for sandstones from different geologic settings, Dvorkin and Nur (1998) ended with the fact that

the medium characteristics are very important controllers on the petrophysical nature of the rocks.

## Conclusions

We collected 40 rock samples from the lower Cretaceous rocks exposed at central Lebanon to study the effects of rock composition and diagenetic processes on their petrophysical properties. Several techniques and measurements were conducted on the collected rock samples including the petrographic investigation and identification of the microfacies, SEM, XRD, porosity, bulk density, and the seismic wave velocities. From the measured petrophysical parameters, we further calculated the grain density and the dynamic elastic constants.

The petrographic investigations revealed that the studied rocks can be categorized into four lithofacies comprising arenitic sandstone, lithic limestone, oolitic limestone, and micritic limestone. The petrographic investigation revealed also that, although dissolution of some clays and feldspar and fracturing may have enhanced the porosity of the studied rock samples, compaction and cementation largely reduced the primary porosity and therefore, the majority of the investigated rock samples possess very low to low porosity.

The petrophysical analyses conducted on the collected core samples revealed that the studied rocks have generally poor porosity (average 6.25%), moderate to high bulk density (average  $2.53 \text{ g/cm}^3$ ), moderate to high  $V_p$  (average 5028 m/s), moderate  $V_s$  (average 2933 m/s), moderate to high elastic moduli (averages of 2.22, 3.59 and  $5.51 \times 10^{10} \text{ Pa}$  for the  $\mu$ ,  $\kappa$ , and  $E$ , respectively), and moderate  $\sigma$  (average 0.24). These values are consistent with the massive and compact nature of most of the studied rocks.

We constructed a number of mutual interrelationships between the measured petrophysical parameters and interpreted them with respect to the rock composition and lithology. The obtained relationships in this study indicate that both porosity and lithology have great effects on the elastic properties of the studied rocks. The fact is also revealed from the observed low  $J$  values after applying the GMR which imply a stronger porosity dependence of the elastic properties of the studied rocks. Moreover, these petrophysical parameters and the seismic wave velocities are controlled mainly by the rock texture, its mineral composition and the subsequent diagenetic processes.

Although many empirical relationships already exist on local, regional, and global scales, they vary from a region to another depending on the physical properties of the sediments of which the rocks are composed, their depositional history, and the geological settings. Our study also

reveals that the investigation of the relationships between porosity and the elastic properties of sedimentary rocks are not easy because the pore geometry, size distribution of pores, and the 3-D pore connectivity are generally very complex. Therefore, a large number of rock samples with known lithology combined with detailed analytical techniques are required to establish strong and more conclusive inferences about these dependent petrophysical properties.

**Acknowledgements** SEM images were taken in the Central Research Science Laboratory/American University of Beirut. The authors thank Ramon Zuniga, Co-Editor-in-chief, *Acta Geophysica*, and two anonymous referees for their critical and fruitful comments which greatly strengthened the manuscript. This research has been partially covered by a Grant from the University Research Board (URB) of the American University of Beirut (Award No. 103009; Project No. 22759).

## References

- Abu Seif ES (2016) Evaluation of geotechnical properties of Cretaceous sandstone, Western Desert, Egypt. *Arab J Geosci* 9:299. <https://doi.org/10.1007/s12517-016-2317-x>
- Adachi T, Sakka S (1990) Dependence of the elastic moduli of porous silica gel prepared by the sol–gel method on heat-treatment. *J Mater Sci* 25(11):4732–4737
- Anselmetti FS, Eberli GP (1999) The velocity-deviation log: a tool to predict pore type and permeability trends in carbonate drill holes from sonic and porosity or density logs. *AAPG Bull* 83(3):450–466
- Ams CH, Knackstedt MA, Pinczewski WV (2002) Accurate  $V_p$ : $V_s$  relationship for dry consolidated sandstones. *Geophys Res Lett*. <https://doi.org/10.1029/2001GL013788>
- Asmani M, Kermel C, Leriche A, Ourak M (2001) Influence of porosity on Young's modulus and Poisson's ratio in alumina ceramics. *J Eur Ceram Soc* 21(8):1081–1086
- Baccelle L, Bosellini A (1965) Diagrammi per la stimaviviva della composizione percentuale nelle rocce sedimentarie. *Ann Univ Ferrara Sezione IX Sci Geol Paleontol* 1:59–62
- Baechle GT, Weger RJ, Massafiero L, Eberli GP (2004) The role of macroporosity and microporosity in constraining uncertainties and in relating velocity to permeability in carbonate rocks. *Society of Exploration Geophysics Extended Abstracts*, vol 23, p 1662
- Baechle GT, Colpaert A, Eberli GP, Weger RJ (2008) Effects of microporosity on sonic velocity in carbonate rocks. *Lead Edge* 27(8):1012–1018
- Bashah NSI, Pierson B (2012) The impact of pore geometry and microporosity on velocity–porosity relationship in carbonates of Central Luconia, Sarawak. Adapted from extended abstract, AAPG international conference on exhibition, Singapore
- Bell FG (1978) The physical and mechanical properties of the fell sandstones, Northumberland, England. *Eng Geol* 12:1–29
- Berge PA, Bonner BP, Berryman JG (1995) Ultrasonic velocity–porosity relationships for sandstone analogs made from fused glass beads. *Geophysics* 60(1):108–119
- Beydoun ZR (1999) Evolution and development of the Levant (Dead Sea Rift) transform system: a historical–chronological review of a structural controversy. In: Mac Niocaill C, Ryan PD (eds) *Continental tectonics, Special publications*, vol 164. Geological Society, London, pp 239–255
- Birch F (1960) The velocity of compressional waves in rocks to 10 kilobar, part 1. *J Geophys Res* 65:1083–1102
- Boisson J, Platon F, Boch P (1976) Measurements of elastic constants and an elastic capacity of some ceramics with various porosities. *Ceramurgia* 6:74–80
- Bou Daher S, Ducros M, Michel P, Hawie N, Nader FH, Littke R (2016) 3-D thermal history and maturity modelling of the Levant Basin and its eastern margin, offshore–onshore Lebanon. *Arab J Geosci* 9:440. <https://doi.org/10.1007/s12517-016-2455-1>
- Burke MM, Fountain DF (1990) Seismic properties of rocks from an exposure of extended continental crust—new laboratory measurements from the Ivrea zone. *Tectonophysics* 182:119–146
- Cadoret T, Marion D, Zinszner B (1995) Influence of frequency and fluid distribution on elastic wave velocities in partially saturated limestones. *J Geophys Res* 100(B6):9789–9803
- Castagna JP, Batzle ML, Eastwood RL (1985) Relationships between compressional wave and shear-wave velocities in clastic silicate rocks. *Geophysics* 50:571–581
- Chen N, Zhu W, Wang TF, Song S (2005) Hydromechanical behavior of country rock samples from the Taiwan Chelungpu Drilling Project, *Eos Trans. AGU* 86(52), Fall meeting supplement, Abstract T51A-1324
- Christensen NI (1974) Compressional wave velocities in possible mantle rocks to pressures of 30 kilobars. *J Geophys Res* 79:407–412
- Christensen NI (1996) Poisson's ratio and crustal seismology. *J Geophys Res* 101(B2):3139–3156
- Daëron M, Klinger Y, Taponnier P, Elias A, Jacques E, Sursock A (2007) 12,000-year-long record of 10 to 13 paleoearthquakes on the Yammouneh fault, Levant fault system, Lebanon. *Bull Seismol Soc Am* 97:749–771
- Dubertret L (1955) Carte géologique du Liban au 1/200000 avec notice explicative. République Libanaise, Ministère des Travaux Publiques, Beirut, p 74
- Dunham RJ (1962) Classification of carbonate rocks according to their depositional texture. In: Ham WE (ed) *Classification of carbonate rocks—a symposium*, vol 1. AAPG Memoir, Tulsa, pp 108–121
- Dunn ML, Ledbetter H (1995) Poisson's ratio of porous and microcracked solids: theory and application to oxide superconductors. *J Mater Res* 10(11):2715–2722
- Dutta T, Mavco G, Mukherji T (2009) Compaction trends for shale and clean sandstone in shallow sediments, Gulf of Mexico. *Lead Edge* 28:590–596
- Dvorkin J, Nur A (1998) Time-average equation revisited. *Geophysics* 63:460–464
- Eberhart-Phillips D, Han DH, Zoback MD (1989) Empirical relationships among seismic velocity, effective pressure, porosity, and clay content in sandstone. *Geophysics* 54:82–89
- Eberli GP, Massafiero JL, Sarg JF (2004) Introduction—seismic images of carbonate reservoirs and systems. In: Eberli GP, Massafiero JL, Sarg JF (eds) *Seismic imaging of carbonate reservoirs and systems*. AAPG Memoir, Tulsa
- Erickson SN, Jarrad RD (1998) Velocity–porosity relationships for water-saturated siliclastic sediments. *J Geophys Res* 103:30385–30406
- Ersoy H, Yalçınalp B, Arslan M, Babacan AE, Çetiner G (2016) Geological and geomechanical properties of the carbonate rocks at the eastern Black Sea Region (NE Turkey). *J Asian Earth Sci* 123:223–233. <https://doi.org/10.1016/j.jafrearsci.2016.07.026>
- Esestine P, Hewitt A, Hodgson N (2016) Zohr—a newborn carbonate play in the Levantine Basin, East-Mediterranean. *First Break* 34:87–93
- Eysa EA, Ramadan FS, El Nady MM, Said NM (2016) Reservoir characterization using porosity–permeability relations and



- statistical analysis: a case study from North Western Desert, Egypt. *Arab J Geosci* 9:403. <https://doi.org/10.1007/s12517-016-2430-x>
- Fabricius IL, Baechle GT, Eberli GP (2010) Elastic moduli of dry and water-saturated carbonates—effect of depositional texture porosity and permeability. *Geophysics* 75(3):N65–N78. <https://doi.org/10.1190/1.3374690>
- Flügel E (1982) *Microfacies analysis of limestone*. Springer, Berlin
- Folk RL (1962) Spectral subdivision of limestone types. In: Ham WE (ed) *Classification of carbonate rocks—a symposium*, vol 1. AAPG Memoir, Tulsa, pp 62–84
- Freund D (1992) Ultrasonic compressional and shear velocities in dry clastic rocks as a function of porosity, clay content, and confining pressure. *Geophys J Int* 108:125–135
- Gardner GHF, Wyllie MRJ, Droschak DH (1965) Hysteresis in the velocity–pressure characteristics of rocks. *Geophysics* 30:111–134
- Gardner GHF, Gardner W, Gregory R (1974) Formation velocity and density—the diagnostic basics for stratigraphic traps. *Geophysics* 39:770–780
- Gardosh M, Garfunkel Z, Druckman Y, Buchbinder B (2010) Tethyan rifting in the Levant region its role in Early Mesozoic crustal evolution. In: Homberg C, Bachmann M (eds) *Evolution of the Levant Margin and Western Arabia Platform since the Mesozoic*, Special publications, vol 341. Geological Society of London, London, pp 9–36
- Garfunkel Z (1989) Tectonic setting of Phanerozoic magmatism in Israel. *Isr J Earth Sci* 38:51–74
- Garfunkel Z (1992) Darfur–Levant array of volcanics—a 140-Ma-long record of hot spot beneath the African–Arabian continent and its bearing on Africa’s absolute motion. *Isr J Earth Sci* 40:135–150
- Gercek H (2007) Poisson’s ratio values for rocks. *Int J Rock Mech Min Sci* 44:1–13. <https://doi.org/10.1016/j.ijrmms.2006.04.011>
- Ghalayini R, Daniel J-M, Homberg C, Nader FH, Comstock JE (2014) Impact of Cenozoic strike-slip tectonics on the evolution of the northern Levant Basin (offshore Lebanon). *Tectonics*. <https://doi.org/10.1002/2014TC003574>
- Gomez F, Khawlie M, Tabet C, Darkal AN, Khair K, Barazangi M (2006) Late Cenozoic uplift along the northern Dead Sea transform in Lebanon and Syria. *Earth Planet Sci Lett* 241:913–931
- Greenfield RJ, Graham EK (1996) Application of the simple relation for describing wave velocity as a function of pressure in rocks containing microcracks. *J Geophys Res* 101:5643–5652
- Han D-H, Batzle M (2004) Gassmann’s equation and fluid-saturation effects on seismic velocities. *Geophysics* 69:398–405
- Han D-H, Nur A, Morgan D (1986) Effects of porosity and clay content on wave velocities in sandstones. *Geophysics* 51(11):2093–2107
- Hawie N, Gorini C, Deschamps R, Nader FH, Montadert L, Grajeon D, Baudin F (2013) Tectono-stratigraphic evolution of the northern Levant Basin (offshore Lebanon). *Mar Pet Geol* 48:392–410
- Hawie N, Deschamps R, Nader FH, Gorini C, Müller C, Desmares D, Hoteit A, Granjeon D, Montadert L, Baudin F (2014) Sedimentologic and stratigraphic evolution of northern Lebanon since the late Cretaceous: implications on the Levant margin and basin. *Arab J Geosci* 7:1323. <https://doi.org/10.1007/s12517-013-0914-5>
- Hyndman RD, Moore G, Moran FK, Hill IA, Taira A, Firth JV et al (1993) Velocity, porosity, and pore-fluid loss from the Nankai Subduction zone accretionary prism. *Proc ODP Sci Results* 131:211–220
- Jeng FS, Weng MC, Lin ML, Huang TH (2004) Influence of petrographic parameters on geotechnical properties of tertiary sandstones from Taiwan. *Eng Geol* 73:71–91
- Ji S (2004) A generalized mixture rule for estimating the viscosity of solid–liquid suspensions and mechanical properties of polyphase rocks and composite materials. *J Geophys Res*. <https://doi.org/10.1029/2004JB003124>
- Ji SC, Wang ZC (1999) Elastic properties of forsterite–enstatite composites up to 3.0 GPa. *J Geodyn* 28:147–174
- Ji SC, Wang Q, Xia B (2002) *Handbook of seismic properties of minerals, rocks and ores*. Polytechnic International Press, Montreal
- Ji S, Wang Q, Xia B (2004) Mechanical properties of multiphase materials and rocks: a simple phenomenological approach using generalized means. *J Struct Geol* 26(8):1377–1390
- Ji S, Gu Q, Xia B (2006) Porosity dependence of mechanical properties of solid materials. *J Mater Sci* 41:1757–1768. <https://doi.org/10.1007/s10853-006-2871-9>
- Ji S, Wang Q, Marcotte D, Salisbury MH, Xu Z (2007) P wave velocities, anisotropy and hysteresis in ultrahigh-pressure metamorphic rocks as a function of confining pressure. *J Geophys Res* 112:B09204. <https://doi.org/10.1029/2006JB004867>
- Ji S, Sun S, Wang Q, Marcotte D (2010) Lamé parameters of common rocks in the Earth’s crust and upper mantle. *J Geophys Res* 115:B06314. <https://doi.org/10.1029/2009JB007134>
- Ji S, Li L, Motra HB, Wuttke F, Sun S, Michibayashi K, Salisbury MH (2018) Poisson’s ratio and auxetic properties of natural rocks. *J Geophys Res*. <https://doi.org/10.1002/2017JB014606>
- Kahraman S, Yeken T (2008) Determination of physical properties of carbonate rocks from P-wave velocity. *Bull Eng Geol Environ* 67:277–281
- Kassab MA, Weller A (2011) Porosity estimation from compressional wave velocity: a study based on Egyptian sandstone formations. *J Petrol Sci Eng* 78:310–315
- Kassab MA, Weller A (2013) Porosity estimation from compressional wave velocity: a study based on Egyptian carbonate samples. *J Earth Sci Eng* 3:314–321
- Kassab MA, Weller A (2015) Study on P-wave and S-wave velocity in dry and wet sandstones of Tushka region, Egypt. *Egypt J Petrol* 24:1–11. <https://doi.org/10.1016/j.ejpe.2015.02.001>
- Kassab MA, Abuseda HH, El Sayed NA, LaLa AM, Elnaggar OM (2016) Petrographical and petrophysical integrated studies, Jurassic rock samples, North Sinai, Egypt. *Arab J Geosci* 9:99. <https://doi.org/10.1007/s12517-015-2146-3>
- Kitamura K, Takahashi M, Masuda K, Ito H, Song S-R, Wang C-Y (2005) The relationship between pore-pressure and the elastic-wave velocities of TCDP-cores. *Eos Trans, AGU*, 86(52), Fall meeting supplement, Abstract T51A-1326, F1833
- Knackstedt MA, Arns CH, Pinczewski WV (2003) Velocity–porosity relationships, 1: accurate velocity model for clean consolidated sandstones. *Geophysics* 68(6):1822–1834. <https://doi.org/10.1190/1.1635035>
- Knackstedt MA, Arns CH, Pinczewski WV (2005) Velocity–porosity relationships: predictive velocity model for cemented sands composed of multiple mineral phases. *Geophys Prospect* 53:349–372
- Longiaru S (1987) Visual comparators for estimating the degree of sorting from plane and thin sections. *J Sedimentol Petrol* 57:792–794
- Marion D, Nur A, Yin H, Han D (1992) Compressional velocity and porosity in sand–clay mixtures. *Geophysics* 57:554–563
- McClusky S, Balassanian S, Barka A, Demir C, Ergintav S, Georgiev I, Gurkan O, Hamburger M, Hurst K, Kahle H, Kastens K, Kekelidze G, King R, Kotzev V, Lenk O, Mahmoud S, Mishin A, Nadariya M, Ouzounis A, Paradissis D, Peter Y, Prilepin M, Reilinger R, Sanli I, Seeger H, Tealeb A, Toksöz MN, Veis G (2000) Global positioning system constrains on plate kinematics and dynamics in the eastern Mediterranean and Caucasus. *J Geophys Res* 105:5695–5719

- McSkimin HJ, Andreatch P, Thurston RN (1965) Elastic moduli of quartz versus hydrostatic pressure at 25 °C and – 195.8 °C. *J Appl Phys* 36(5):1624–1632. <https://doi.org/10.1063/1.1703099>
- Mousa AS, El-Hariri TYMA, Abu Assy EMA (2011) Sedimentological and petrophysical characteristics of Raha Formation at Wadi Tubia, Northern Gulf of Aqaba, Sinai, Egypt. *Egypt J Petrol* 20:79–87. <https://doi.org/10.1016/j.ejpe.2011.06.003>
- Müller C, Higazi F, Hamdan W, Mroueh M (2010) Revised stratigraphy of the upper Cretaceous and Cenozoic series of Lebanon based on nanofossils, Special publications, vol 341. Geological Society of London, London, pp 287–303
- Nabawy BS, Barakat MKh (2017) Formation evaluation using conventional and special core analyses: Belayim Formation as a case study, Gulf of Suez, Egypt. *Arab J Geosci* 10:25. <https://doi.org/10.1007/s12517-016-2796-9>
- Nabawy BS, David C (2016) X-ray CT scanning imaging for the Nubia sandstone as a tool for characterizing its capillary properties. *Geosci J* 20:691–704. <https://doi.org/10.1007/s12303-015-0073-7>
- Nabawy BS, Sediek KN, Nafee SA (2015) Pore fabric assignment using electrical conductivity of some Albian–Cenomanian sequences in north Eastern Desert, Egypt. *Arab J Geosci* 8:5601–5615. <https://doi.org/10.1007/s12517-014-1631-4>
- Nader FH (2014) The geology of Lebanon. Scientific Press, London, p 108
- Nanda N (2016) Seismic data interpretation and evaluation for hydrocarbon exploration and production. Springer, Berlin. <https://doi.org/10.1007/978-3-319-26491-2>. ISBN 978-3-319-26489-9
- Ngoc NH, Aziz SB, Duc NA (2014) The application of seismic attributes for reservoir characterization in pre-tertiary fractured basement, Vietnam–Malaysia offshore. *Interpretation* 2(1):SA57–SA66. <https://doi.org/10.1190/INT-2013-0081.1>
- Nur A, Mavko G, Dvorkin J, Gal D (1995) Critical porosity: the key to relating physical properties to porosity in rocks. 65th SEG meeting, Houston, USA, Expanded abstracts
- Ojha M, Sain K (2014) Velocity–porosity and velocity–density relationship for shallow sediments in the Kerala–Konkan Basin of western Indian margin. *J Geol Soc India* 84:187–191
- Onajite E (2014) Seismic data analysis techniques in hydrocarbon exploration. Elsevier, Amsterdam. <https://doi.org/10.1016/C2013-0-09969-0>
- Panakkal JP, Willems H, Arnold W (1990) Nondestructive evaluation of elastic parameters of sintered iron powder compacts. *J Mater Sci* 25(2):1397–1402
- Porter DF, Reed JS, Lewis D III (1977) Elastic moduli of refractory spinels. *J Am Ceram Soc* 60(7–8):345–349
- Rafavich F, Kendall CH, Todd TP (1984) The relationship between acoustic properties and the petrographic character of carbonate rocks. *Geophysics* 49:1622–1636
- Raymer LL, Hunt ER, Gardner JS (1980) An improved sonic transit time-to-porosity transform. *Trans SPWL Annu Logging Symp* 13:133–152
- Russell BH, Smith T (2007) The relationship between dry rock bulk modulus and porosity—an empirical study. *CREWES Res Rep* 19:1–14
- Salem HS (2000) Poisson’s ratio and the porosity of surface soils and shallow sediments, determined from seismic compressional and shear wave velocities. *Géotechnique* 50(4):461–463
- Scholle PA, Ulmer-Scholle DS (2003) A color guide to the petrography of carbonate rocks: grains, textures, porosity, diagenesis, vol 77. AAPG Memoir, Tulsa
- Schön JH (1996) Physical properties of rocks: fundamentals and principles of petrophysics. Elsevier, Oxford
- Selley RC, Sonnenberg SA (2015) Elements of petroleum geology, 3rd edn. Academic Press, Elsevier
- Shakoor A, Bonelli RE (1991) Relationship between petrographic characteristics, engineering index properties, and mechanical properties of selected sandstones. *Bull Assoc Eng Geol* 28(1):55–71
- Sharma PK, Singh TN (2008) A correlation between P-wave velocity, impact strength index, slake durability index and uniaxial compressive strength. *Bull Eng Geol Environ* 67:17–22. <https://doi.org/10.1007/s10064-007-0109-y>
- Singh TN, Kanchan R, Saigal K, Verma AK (2004) Prediction of P-wave velocity and anisotropic property of rock using artificial neural network technique. *J Sci Ind Res* 63(1):32–38
- Soga N, Schreiber E (1968) Porosity dependence of sound velocity and Poisson’s ratio for polycrystalline MgO determined by resonant sphere method. *J Am Ceram Soc* 51(8):465–467
- Sønneland L, Barkved O (1990) Use of seismic attributes in reservoir characterization. In: Buller AT, Berg E, Hjelmeland O, Kleppe J, Torsæter O, Aasen JO (eds) North Sea oil and gas reservoirs—II. Springer, Dordrecht. [https://doi.org/10.1007/978-94-009-0791-1\\_8](https://doi.org/10.1007/978-94-009-0791-1_8)
- Stewart RR, Gaiser JE, Brown RJ, Lawton DC (2000) Converted-wave seismic exploration: applications. *CREWES Res Report*, vol 12
- Sun S, Ji S, Wang Q, Salisbury M, Kern H (2012) P-wave velocity differences between surface-derived and core samples from the Sulu ultrahigh-pressure terrane: implications for in situ velocities at great depths. *Geology* 40(7):651–654
- Tatar O, Piper JDA, Gürsoy H, Heimann A, Koçbulut F (2004) Neotectonic deformation in the transition zone between the Dead Sea Transform and the East Anatolian Fault Zone, Southern Turkey: a palaeomagnetic study of the Karasu Rift Volcanism. *Tectonophysics* 385:17–43. <https://doi.org/10.1016/j.tecto.2004.04.005>
- Timoshenko SP, Goodier JN (1970) Theory of elasticity, 3rd edn. McGraw-Hill, New York
- Tucker ME, Wright VP (1990) Carbonate sedimentology. Blackwell Scientific, Oxford
- Ulusay R, Tureli K, Ider MH (1994) Prediction of engineering properties of selected litharenite sandstone from its petrographic characteristics using correlation and multivariate statistical techniques. *Eng Geol* 37:135–157
- Vernik L, Fisher D, Bahret S (2002) Estimation of net-to-gross from P and S impedance in deepwater turbidites. *Lead Edge* 21:380–387
- Walley CD (1983) A revision of the lower Cretaceous stratigraphy of Lebanon. *Geol Rundsch* 72(1):377–388
- Walley CD (1997) The lithostratigraphy of Lebanon: a review. *Leban Sci Bull* 10:1
- Walley CD (1998) Some outstanding issues in the geology of Lebanon and their importance in the tectonic evolution of the Levantine region. *Tectonophysics* 298:37–62. [https://doi.org/10.1016/S0040-1951\(98\)00177-2](https://doi.org/10.1016/S0040-1951(98)00177-2)
- Wang Z (2000) Velocity–density relationships in sedimentary rocks. In: Wang Z, Nur A (eds) Seismic and acoustic velocities in reservoir rocks: recent developments, vol 3. Society of Exploration Geophysics, Tulsa, pp 258–268
- Wang Q, Ji S (2009) Poisson’s ratio of crystalline rocks as a function of hydrostatic confining pressure. *J Geophys Res*. <https://doi.org/10.1029/2008JB006167>
- Wang Z, Nur A (1992) Aspect of rock physics in seismic reservoir surveillance. In: Sheriff RE (ed) Reservoir geophysics. Society of Exploration Geophysicists, Tulsa, pp 285–300
- Wang J-H, Hung J-H, Dong J-J (2009) Seismic velocities, density, porosity, and permeability measured at a deep hole penetrating the Chelungpu fault in central Taiwan. *J Asian Earth Sci* 36:135–145. <https://doi.org/10.1016/j.jseae.2009.01.010>

- Weger RJ, Eberli GP, Baechle GT, Massafiero JL, Sun YF (2009) Quantification of pore structure and its effect on sonic velocity and permeability in carbonates. *AAPG Bull* 93(10):1–21
- Wepfer WW, Christensen NI (1991) A seismic velocity–confining pressure relation, with applications. *Int J Rock Mech Min Sci Geomech Abstr* 28:451–456
- Wilson JL (1975) *Carbonate facies in geologic history*. Springer, New York
- Wilson M (1992) Magmatism and continental rifting during the opening of the South Atlantic Ocean: a consequence of lower Cretaceous super-plume activity. In: Storey BC, Alabaster T, Pankhurst RJ (eds) *Magmatism and the causes of continental breakup*, Special publications, vol 68. Geological Society of London, London, pp 241–255
- Winkler KW, Murphy WF III (1995) Acoustic velocity and attenuation in porous rocks. *Rock physics and phase relations: a handbook of physical constants*. AGU, Washington, pp 20–34
- Wyllie MRJ, Gregory AR, Gardner LW (1956) Elastic wave velocities in heterogeneous and porous media. *Geophysics* 21:41–70
- Wyllie MRJ, Gregory AR, Gardner GHF (1958) An experimental investigation of factors affecting elastic wave velocities in porous media. *Geophysics* 23:459–493
- Xu S, White RE (1995) A new velocity model for clay–sand mixtures. *Geophys Prospect* 43:91–118
- Yehekel O, Shokhat M, Ratzker M, Dariel MP (2001) Elastic constants of porous silver compacts after acid assisted consolidation at room temperature. *J Mater Sci* 36(5):1219–1225
- Yu C, Ji S, Li Q (2016) Effects of porosity on seismic velocities, elastic moduli and Poisson’s ratios of solid materials and rocks. *J Rock Mech Geotech Eng* 8:35–49. <https://doi.org/10.1016/j.jrmge.2015.07.004>